Redox proteome analysis of auranofin exposed ovarian cancer cells (A2780)

Giovanni Chiappetta, Tania Gamberi, Fiorella Faienza, Xhesika Limaj, Salvatore Rizza, Luigi Messori, Giuseppe Filomeni, Alessandra Modesti, Joelle Vinh

Redox proteome analysis of auranofin exposed ovarian cancer cells (A2780)

Article *in* Redox Biology · March 2022

DOI: 10.1016/j.redox.2022.102294

9 authors, including:

Giovanni Chiappetta
École Supérieure de Physique et de Chimie Industrielles-CNRS
48 PUBLICATIONS **479** CITATIONS
SEE PROFILE

Tania Gamberi
University of Florence
80 PUBLICATIONS **1,034** CITATIONS
SEE PROFILE

Salvatore Rizza
Danish Cancer Society
38 PUBLICATIONS **914** CITATIONS
SEE PROFILE

Luigi Messori
University of Florence
413 PUBLICATIONS **14,622** CITATIONS
SEE PROFILE

Redox Biology 52 (2022) 102294

Contents lists available at ScienceDirect

Redox Biology

journal homepage: www.elsevier.com/locate/redox

Redox proteome analysis of auranofin exposed ovarian cancer cells (A2780)

Giovanni Chiappetta [a,*], Tania Gamberi [b,**], Fiorella Faienza [c], Xhesika Limaj [a], Salvatore Rizza [d], Luigi Messori [e], Giuseppe Filomeni [c,d,f], Alessandra Modesti [b], Joelle Vinh [a]

[a] Biological Mass Spectrometry and Proteomics Group, SMBP, PDC CNRS UMR, 8249, ESPCI Paris, Université PSL, 10 rue Vauquelin, 75005, Paris, France
[b] Department of Experimental and Clinical Biomedical Sciences, University of Florence, Viale G.B. Morgagni 50, 50134, Florence, Italy
[c] Department of Biology, University of Rome Tor Vergata, Rome, Italy
[d] Redox Signaling and Oxidative Stress Group, Danish Cancer Society Research Center, Copenhagen, Denmark
[e] Metmed Lab, Department of Chemistry, University of Florence, via della lastruccia 3, 50019, Sesto Fiorentino, Italy
[f] Center for Healthy Aging, University of Copenhagen, Denmark

ARTICLE INFO

Keywords:
Redox proteomics
Cysteine
Auranofin
Gold drugs
Ovarian cancer

ABSTRACT

The effects of Auranofin (AF) on protein expression and protein oxidation in A2780 cancer cells were investigated through a strategy based on simultaneous expression proteomics and redox proteomics determinations. Bioinformatics analysis of the proteomics data supports the view that the most critical cellular changes elicited by AF treatment consist of thioredoxin reductase inhibition, alteration of the cell redox state, impairment of the mitochondrial functions, metabolic changes associated with conversion to a glycolytic phenotype, induction of ER stress. The occurrence of the above cellular changes was extensively validated by performing direct biochemical assays. Our data are consistent with the concept that AF produces its effects through a multitarget mechanism that mainly affects the redox metabolism and the mitochondrial functions and results into severe ER stress. Results are discussed in the context of the current mechanistic knowledge existing on AF.

1. Introduction

Auranofin [2,3,4,6-tetra-*O*-acetyl-l-thio-β-D-glycopyranosato-S-(triethyl-phosphine)-gold] (AF), first developed in the late 1970s [1], is a linear Au(I) complex containing an Au–S bond that is further stabilized by gold(I) coordination to a triethyl phosphine group. Auranofin was approved in 1985 by Food and Drug Administration (FDA), USA, to treat rheumatoid arthritis under the proprietary name Ridaura® [2].

In recent years, AF has been intensely investigated for new potential therapeutic applications in several diseases related to viral [3] parasitic [4], fungal [5] and bacterial [6] infections, in neurodegenerative disorders [7] and cancer [8,9]. Concerning cancer, AF was found to exhibit a relevant cytotoxic activity *in vitro* against several types of human cancer cell lines [10–14] and a remarkable efficacy against a few *in vivo* models [15,16].

The anti-inflammatory and anti-cancer activities of AF have been studied in great detail in many laboratories. However, its exact mechanism of action is yet to be proved [7,9]. In this regard, we like reminding that deciphering the mechanism of action of metallodrugs is a highly challenging task due to the usually broad reactivity of such compounds, often transforming them into a variety of bioactive metabolites within the biological milieu. Among the several formed metallo-metabolites, only a few are biochemically and functionally relevant for the reported *in vitro* and *in vivo* effects [17].

Even though the metabolism of AF has not been elucidated conclusively, there is a large consensus that, upon activation, the sugar thiolate is released from gold(I) coordination; this process results in the formation of the triethylphosphine gold $[Au(PEt3)]^+$ cation, a metabolite responsible for cellular target binding and redox-dependent effects [18,19]. Furthermore, AF, like most gold complexes, manifests a great reactivity towards free selenocysteine (Sec) or cysteine (Cys) residues [20,21]. Accordingly, the pharmacological actions of AF were mainly traced back to inhibition of cytosolic and mitochondrial thioredoxin reductase (TrxR1 and TrxR2), two selenoenzymes essential for the Thioredoxin (Trx) pathway, which regulates the intracellular redox homeostasis [22,23] by thiol chemistry. Strong inhibition of these selenoenzymes leads to a large increase in cellular oxidative stress and intrinsic apoptosis [13,18,24,25] by mitochondrial swelling and loss of

* Corresponding author.
** Corresponding author.
E-mail addresses: giovanni.chiappetta@espci.fr (G. Chiappetta), tania.gamberi@unifi.it (T. Gamberi).

https://doi.org/10.1016/j.redox.2022.102294
Received 1 March 2022; Accepted 16 March 2022
Available online 22 March 2022

mitochondrial membrane potential followed by caspase-3 and caspase-9 activation [11,24]. Angelucci et al. proposed a model for the mechanism of AF inhibition [26], wherein the gold center is first displaced from the S-glucosyl ligand by the nucleophilic attack of the TrxR-Sec group. Then gold is transferred from the Sec-group to the catalytic cysteines inhibited by forming a Cys-Au-Cys adduct. This mechanism would imply that TrxR Sec-group could transfer the gold-moiety also to other less reactive protein targets. Additional cellular targets and mechanisms of action have been proposed so far for AF. Notably, AF was also found to inhibit several pro-inflammatory pathways, including NF-κB, signal transducer and activator of transcription (STAT)-3, Toll-like receptor (TLR) signalling, and angiogenesis [27–29].

Currently, in the frame of the so-called "drug repurposing" strategies, AF is in clinical trials for the treatment of chronic lymphocytic leukaemia (clinicaltrials.gov/ct2/show/NCT01419691), lung (clinicaltrials.gov/ct2/show/NCT01737502), and ovarian cancer (clinicaltrials.gov/ct2/show/NCT01747798). In ovarian cancer (OC), several studies provided evidence of AF efficacy and its ability to overcome cisplatin resistance [10,11,30]. Schuh et al. [30] confirmed that in human OC cells sensitive (A2780) and resistant (A2780/R) to cisplatin, the antiproliferative properties of this gold(I) compound are mainly due to direct inhibition of TrxR enzymes. AF was also reported to be very effective in BRCA1-defective ovarian cells due to the accumulation of unrepaired DNA damage [31]. Importantly, substantial evidence has been gained demonstrating the synergistic enhancement of AF effects when combined with other compounds, thereby providing a rationale to reposition the FDA-approved drug AF for cancer therapy [13,32].

In recent years, mass spectrometry-based proteomics has become a powerful and systematic tool for large-scale protein identification of metal-based anti-cancer drug mechanisms and the associated drug-protein interactions [33,34]. In this frame, a few proteomic studies have been carried out so far to unveil the anti-cancer mode of action of AF. Our research group exploited the classical proteomic method based on joint two-dimensional electrophoresis (2DE) and mass spectrometry (MS) analysis, to single out the molecular mechanisms through which AF produces its biological effects in human ovarian cancer cells either sensitive (A2780) or resistant (A2780/R) to cisplatin. We could demonstrate the direct involvement of oxidative stress in AF cytotoxicity in A2780 sensitive cells; at variance, in the case of A2780/R cells, we pointed out that AF mainly acts by altering the proteasome proteins expression [35,36]. Likewise, Zhang et al. demonstrated through a shotgun proteomic approach that in HCT116 colon carcinoma cells, TrxR inhibition is the primary mode of action of AF while proteasome inhibition is just an off-target effect [25]. Besides, Hatem et al., applying a SILAC-based proteomics strategy, confirmed that AF, alone and in combination with vitamin C, targeted both glutathione and thioredoxin systems in lung and breast cancer cells [37].

To the best of our knowledge, only two studies so far dealt with MS-based cysteine redox proteomics to analyse the mode of action of AF. First in chronological order, Go et al. employed redox ICAT (Isotope Coded Affinity Tag)-combined mass spectrometry to examine the effect of AF on the cysteine proteome and reported that the identified oxidized peptides were primarily involved in glycolysis, cytoskeleton remodeling, translation, and cell adhesion [38]. More recently, Saei et al. attempted to find the AF protein targets by an innovative chemical proteomic approach, combining the techniques of Thermal Proteome Profiling (TPP), Functional Identification of Target by Expression Proteomics (FITExP), and cysteine redox proteomics. They confirmed TrxR1 as one of the main AF targets. Moreover, they identified NFKB2 (Nuclear factor NF-kappa-B p100 subunit) and CHORDC1 (Cysteine and histidine-rich domain-containing protein 1) as novel AF targets [39]. Thus, in this study, cysteine redox proteomics was exploited to find candidate cysteine ligands of gold rather than to highlight the effects of AF on the cysteine redox balance. Overall, the above observations suggest for a complex and multifactorial Auranofin mode of action that warrants further investigations. In the attempt to address this issue, we considered that an unbiased proteomics study using more recent technologies could help in expanding the comprehension of AF effects in cancer cells. Thus, our study aims to generate data-driven hypotheses to disclose new aspects or discover incremental details of already known mechanisms of AF cytotoxicity and of cell adaptation to this drug, together with more fundamental topics of thiol biology. More in detail, in this work we explored the effects of direct exposure to AF, in the A2780 ovarian cancer cell model, monitoring protein and cysteine oxidation levels by a label-free redox proteomics strategy based on the biotin switch technique. Compared to the ICAT-based study performed by Go et al. [39], our approach provides an additional point of view, allowing us to correlate protein expression changes with cysteine oxidations. Subsequent Bioinformatics analysis disclosed a set of cellular processes most probably affected by the treatment. In this article, in particular, we offer a comprehensive interpretation of the redox proteomics dataset validating the most relevant results by direct biochemical assays.

2. Materials and methods

2.1. Cell line and culture conditions

The human ovarian cancer cell line A2780 was purchased from the European Collection of Authenticated Cell Cultures (ECACC, a part of Public Health England) (Lot Nº 13J012, Sigma Aldrich). Cells were maintained in RPMI1640 medium supplemented with 10% FBS, 1% glutamine, and antibiotics (penicillin, 100 U/ml; streptomycin, 100 μg/ml) at 37 °C in a 5% CO2 humidified atmosphere and subcultured twice weekly.

Wild Type (WT) and C501S TRAP1 mutant were synthesized and cloned in pcDNA3.1 (+)-C-HA vector using the Gene Synthesis & DNA Synthesis service from GeneScript Biotec.

For WT and C501S TRAP1 expression, A2780 cells were transiently transfected with Lipofectamine 2000, and the experiments were performed 48 h post-transfection.

2.2. Cell viability

Auranofin (Sigma Aldrich Merck) was dissolved in DMSO (Dimethyl sulfoxide) to obtain a stock solution of 20 mM.

Standard MTT (4,5-dimethylthiazol-2-yl]-2,5 diphenyl tetrazolium bromide) proliferation assay was used to determine the effect of AF on A2780 cell viability. Exponentially growing cells were seeded in 96-well microplates in RPMI 1640 supplemented with 10% FCS at a density of 8x103. After 24 h, 0.7 μM of Auranofin (corresponding to the previously calculated 72-h-exposure IC_{50}-dose) [11,40] was added in a fresh RPMI medium and incubated for 6, 12, 24, 48 and 72 h. At the end of incubation, cells were treated for 1 h at 37 °C with 0.5 mg/ml MTT dissolved in PBS. Then, MTT was removed, cells were washed in PBS and 100 μl of stop solution (DMSO) were added. After 15 min of incubation at 37 °C, optical density was read in the microplate reader interfaced with the software Microplate Manager/PV version 4.0 (Bio-Rad Laboratories) at 595 nm. Cell death in the experiments with C501S TRAP1 mutant was determined after 24 h of AF treatment by flow cytometry (FACS Celesta, BD) after Propidium Iodide (Sigma-Aldrich) staining, measuring the SubG1 cell fraction.

2.3. Drug treatment

Exponentially growing cells were seeded in three 60 mm^2 Petri dishes at a density of $1x10^6$/dish. After 24 h, 0.7 μM of (corresponding to the previously calculated 72-h-exposure IC_{50}-dose) [11,40] was added in a fresh RPMI medium and incubated for different times depending on the selected experiments. At the end of incubation, cells were washed at least three times with phosphate-buffered saline solution (PBS) and then lysed in appropriate buffers for the selected analysis. The A2780 control

cells were treated in triplicate with an equal volume of DMSO.

2.4. TrxR enzymatic activity inhibition assay

After treatment with 0.7 μM of Auranofin for 6, 12, 24 h, A2780 cells were lysed with RIPA buffer (50 mM Tris-HCl pH 7.5, 150 mM NaCl, 100 mM NaF, 2 mM EGTA, 1% Triton X-100) containing 10 μl/ml protease and phosphatase inhibitors (Sigma Aldrich). Lysates were centrifugated at 4 °C, 14,000 RPM for 15 min, and supernatants were collected. After protein quantification with Bradford Assay, 30 μg of proteins were used for the assay. TrxR activity was measured by using a commercial colorimetric assay kit (Sigma Aldrich CS0170) based on the reduction of 5,5′-dithiobis (2-nitrobenzoic acid) (DTNB) with NADPH to 5-thio-2-nitrobenzoic acid (TNB) at 412 nm. This kit also contains a solution of mammalian TrxR inhibitor. Experiments were performed in triplicate. Results were normalized to the cellular protein content and reported as the percentage of enzyme activity compared to the untreated (control) cells.

2.5. Redox proteomics sample preparation

After 24 h of treatment with 0.7 μM of Auranofin, an equal number of control and AF-treated A2780 ovarian cancer cells ($2x10^6$) were lysed by sonication using trichloroacetic acid (TCA in water, 20% w:v, Sigma-Aldrich Merck) in a wet ice bath. Three biological replicates were used for each condition. After centrifugation (30 min, 4 °C, 13,000 RPM) and three acetone washes, the protein pellets were resuspended in 600 μL of a denaturing solution: 6 M Urea (Sigma-Aldrich Merck), 150 mM Tris pH 8.5 (Sigma Aldrich Merck), β-octyl-glucopyranoside 1% (Sigma Aldrich Merck), protease inhibitors (Complete, Roche), 200 mM of iodoacetamide (IAM, Sigma-Aldrich Merck) and allowed to react for 1 h at 37 °C under stirring to ensure the reduced thiol saturation as we showed in previous works [41,42]. Total protein concentration was estimated by a colorimetric assay (BCA Protein Assay Kit, Pierce) and adjusted for each sample at 1 μg/μL. Proteins were precipitated with TCA and washed with acetone to remove IAM, then incubated in the denaturing solution supplemented with 20 mM of dithiothreitol (DTT) for 2 h at 37 °C. Proteins were precipitated with TCA, washed with acetone to remove DTT, then incubated in denaturing solution supplemented with 0.4 mM of EZ-Link HPDP-biotin (from 4 mM stock solution, Thermo Scientific) for 1 h at 37 °C forming a mixed disulfide-bond with the newly generated thiols. Proteins were precipitated with TCA, washed with acetone to remove HPDP-biotin, then enzymatically proteolyzed overnight at 37 °C with 1 μg of trypsin/Lys-C (Promega) in 50 mM ammonium bicarbonate solution (AMBIC, Sigma-Aldrich Merck). Biotinylated peptides were enriched on a streptavidin resin (High capacity, Thermo Scientific) by incubation for 30 min at rt. Unretained species were recovered by centrifugation (1 min, 2,000 RPM). Biotinylated enriched fractions were eluted by cleaving the biotin moiety with a solution of 10 mM AMBIC, 10 mM of DTT and incubating the resin at rt for 30 min. Both unbound and eluted fractions were acidified with trifluoroacetic acid (TFA, final concentration0.1% v:v) and stored at 4 °C in glass vials for LC-MS/MS.

2.6. Mass spectrometry

For each sample fraction 6 μL of sample was pre-concentrated on a C18 cartridge (Dionex Acclaim PepMap100, 5 μm, 300 μm i.d. x 5 mm) and eluted on a capillary reverse-phase column (C18 Dionex Acclaim PepMap100, 3 μm, 75 μm i.d. x 50 cm) at 220 nL/min, with a gradient of 2%–50% of buffer B in 120 min for the bound fractions and 180 min for the unbound fractions; (A: 0.1% aq. Formic Acid/Acetonitrile 98:2 (v/v); B: 0.1% aq. Formic Acid/Acetonitrile 10:90 (v/v)), coupled to a quadrupole-Orbitrap mass spectrometer (Q Exactive HF, ThermoFisher Scientific) using a Top 20 data-dependent acquisition MS experiment: 1 survey MS scan (400-2,000 *m/z*; resolution 70,000) followed by 20 MS/MS scans of the 20 most intense precursors (dynamic exclusion of 30 s, resolution 17,500).

2.7. Data processing

LC-MS/MS data were processed with Protein Discoverer 2.4.0 (Thermo Scientific). Streptavidin bound and unbound fractions were submited to two independent database searches. Protein identification was performed with Mascot (Matrix Science) and Sequest™ HT (Thermo Scientific) search engines against the SwissProt sequence database (01/2020 version) with a mass tolerance at 10 ppm for MS and 0.02 Da for MS/MS data. Trypsin digestion was set allowing up to 3 miscleavages. Met oxidation, Asn and Gln deamidations, and Cys carbamidomethylation were set as variable modifications. Peptide Spectrum Matches (PSMs) were filtered using a False Discovery Rate (FDR) of 0.01, calculated with a concatenated target-decoy database. Cys-containing peptides for redox proteomics were considered if the associated Post Error Probability (PEP) value was lower than 0.01. Protein identifications and quantifications were realized with the peptides detected in both streptavidin bound and unbound fractions. Peptide intensities of the streptavidin bound and unbound datasets were independently normalized and scaled using the total ion current of the most intense LC-MS/MS run as reference. The streptavidin bound and unbound search outputs were then merged, and protein quantification was recalculated in label-free mode using the three most intense peptides, excluding the cysteine containing peptides. Protein and peptide MS intensities were converted in Log2. The fold changes were calculated in Log scale (Log2) as differences between the median MS intensities of the AF-treated and untreated cell biological replicates. For each fold change, a Z-score was calculated according to the equation:

$$Z = \frac{|D_i - \overline{D}|}{\sigma}$$

With D*i*: difference for a given protein, $\overline{D}$: the mean difference of all protein ratios of the dataset, σ: standard deviation of all protein differences calculated in the dataset.

A Student's test was performed using the normalized median protein intensities and their respective variances to find significant protein expression changes. Proteins exhibiting a p-value$<$0.05 and Z-score$>$1 were considered significant. Proteins detected in 2/3 biological replicates in the AF treated samples and undetected in control (untreated) samples were considered upregulated. Vice versa, proteins detected in 2/3 biological replicates in control (untreated) samples and undetected in the AF treated samples were considered downregulated.

To find significant changes in Cys oxidation/reduction levels and to avoid the bias of protein expression we used a different approach. Peptides containing reduced Cys (carbamidomethylated) were recovered from the bound and unbound fractions while, peptide containing initially oxidized Cys (detected in the final reduced form because of the cleavage of the biotin in the elution step) were recovered from the bound fraction only. The fold changes of the Cys-containing peptides were calculated as the difference between the median MS intensities (Log2) of the AF treated and control samples. Then, the Cys-containing peptide fold changes and the associated variances were compared by a Student's test to the correspondent protein fold change and associated variance to find significant differences. If the Cys containing peptide fold changes deviate from the related protein fold change, it was considered a significant change of the Cys redox fraction. Thus, the normalized peptide fold changes (*N*) were calculated as follows:

$$N = \log 2\left(\frac{I_{cysAF}/I_{protAF}}{I_{cysCTR}/I_{protCTR}}\right)$$

where *I* is the median intensity and the subscripts indicate the sample

type (*cys*: Cys-containing peptide, *AF*: Auranofin-treated cells, *prot*: protein, *CTR*: untreated cells).

A Z-score was calculated as previously described but using the values *N*. Cys-containing peptides exhibiting p-value< 0.05 and Z-score>1 were considered significant.

2.8. Data availability

The mass spectrometry proteomics data have been deposited to the ProteomeXchange Consortium via the PRIDE partner repository with the dataset identifier PXD028681.

2.9. Bioinformatic analysis

The lists of the upregulated and downregulated proteins were separately submitted to the bioinformatics platform DAVID [43] for the gene ontology (GO) enrichment analysis. Biological Process (GOBP) and Kegg's Pathway results were exported. In order to overcome the bias of the intrinsic selectivity of the protein extraction protocols [44] on GO enrichment, the whole dataset of the detected proteins was submitted to DAVID as a background list. Thus, for each GOBP/Kegg's pathway output, an enrichment fold change was calculated as the ratio between the number of enriched proteins in the downregulated/upregulated datasets and the number of enriched proteins in the background dataset. GOBP/Kegg's pathway outputs showing fold changes greater than 2 and enrichment p-values < 0.01 were considered.

The dataset combining upregulated and downregulated proteins was submitted to Ingenuity Pathway Analysis (IPA, QIAGEN). To the proteins detected only in the AF treated cells a fold change +10 was attributed, while to the protein detected exclusively in the control a fold change −10 was attributed.

We used the Protein Data Bank (PDB) codes for proteins showing increased levels of oxidized form and decreased levels of reduced form for the Cpipe analysis on the cysteine chemical features (bioinformatics.akdeniz.edu.tr/cpipe/start.py), generating two test datasets. We created a background dataset (control) containing the PDB codes of all the detected proteins. This was also submitted to Cpipe to highlight eventual enrichments of chemical/physical features of the oxidized cysteines. The monitored chemical/physical parameters in Cpipe are reported as scores ranging from 0 (lowest) to 1 (highest). For each monitored Cpipe feature, the percentage of cysteine residues in the dataset showing a score >0.75 was calculated.

2.10. Biochemical analyses

The biochemical analysis was performed in the same experimental condition of the proteomics studies. The Oxygen Consumption Rate (OCR) analysis was performed using a Clark-type O2 electrode inserted in a thermostatic airtight chamber (Oxygraph Plus System, Hansatech Instruments). Briefly, control and treated cells were trypsinized, washed with PBS, and suspended in a culture medium at the concentration of 10^6 cells/mL. To measure the steady-state OCR,1 ml of cell suspension was transferred to the airtight chamber maintained at 37 °C, and oxygen consumption was monitored for 10 min. The OCR values were normalized from the total protein of each sample (nmol of consumed O_2/mg of protein) and reported as the percentage of OCR relatively to control cells.

Lactate amounts of cell culture media coming from untreated and treated cells were measured with the K-LATE kit (Megazyme) according to the datasheet provided by the manufacturer. Lactate content was normalized to the total protein of each sample (mmoles of produced lactate/mg of protein) and reported as the percentage of lactate production with respect to untreated cells.

2.11. Western blot

Cells were cultured and treated in the same manner as for the proteomics. Afterward, cells were lysed in RIPA buffer containing 10 μl/ml protease and phosphatase inhibitors (Sigma Aldrich). Lysates were centrifugated at 4 °C, 14,000 rpm for 15 min, and supernatants were collected. After protein quantification with Bradford Assay, 20 μg of proteins were separated on 4–20% pre-cast SDS-PAGE (Bio-Rad Laboratories) and blotted onto PVDF membranes (Bio-Rad Laboratories). Primary antibodies of complex I (subunit NDUFB8) mitochondrial enzyme (AbCam, ab110242), complex III (subunit UQCRC2) mitochondrial enzyme (AbCam, ab14745), complex IV (subunit MTCO1) mitochondrial enzyme (AbCam, ab14705), complex V (subunit ATP5A) mitochondrial enzyme (AbCam, ab14748), Bcl-2 (Santa Cruz, sc-7382), Bax (Santa Cruz, sc-7480), Ubiquitin (Santa Cruz, sc-8017), PARP1 (Enzo Life Science, BML-SA249-0050), Trap1 (Santa Cruz, sc-13557), LDH (Santa Cruz, sc-133123) were added (1:1,000) to a 2% non-fat dry milk in PBS tween solution. PVDF membranes were incubated overnight at 4 °C. Then membranes were treated with Horseradish peroxidase (HRP)-conjugated secondary antibodies (Santa Cruz), and bands were immunodetected with enhanced chemiluminescence (ECL) kit detection system (GE Healthcare) at Amersham Imager 600. For the quantification, densitometric analysis of the bands was performed using ImageJ2 software version 2.0.0-rc-64, and the intensities of the immune-stained bands were normalized on the respective Coomassie-stained PVDF membrane.

2.12. Statistical analysis

The non-proteomic experiments were carried out, at least, in triplicate (three independent experiments). Statistical analysis was performed by a two-tailed T-test or by one-way ANOVA test followed by Tuckey's multiple comparisons test using Graphpad Prism 6. A p-value$\leq$0.05 was considered statistically significant. Results were reported as mean ± SD.

3. Results and discussion

3.1. Expression and redox proteomics: global results

A2780 ovarian cancer cells were exposed to AF 0.7 μM for 24 h. Our previous studies showed that this concentration corresponds to the 72 h-exposure IC_{50}-dose in A2780 cells [11,40]. Here we show that at this exposure condition, cells were viable (Fig. 1A), obtaining an inhibition of the TrxR activity of about 50% (Fig. 1B). Since TrxR is considered to be the primary target of AF, we applied this exposure condition to improve the understanding of the importance of its enzymatic inhibition in the AF mode of action. Hence, after 24 h of treatment, control (untreated) and AF-exposed A2780 cells were submitted to a redox proteomics workflow based on a biotin-switch approach in label-free quantification mode (Fig. 2). Protein profiles were calculated using the Cys-free peptides detected by LC- MS/MS analysis. About 3,200 proteins were quantified, and 438 were found upregulated, while 222 were downregulated (Fig. 3, Supplementary Table 1). Moreover, 86 proteins were detected only in the AF-treated sample, while 5 were only detected in the untreated sample. The lists of upregulated and downregulated proteins were separately submitted to the bioinformatics tool DAVID [43] to perform the gene ontology enrichment analysis. The biological functions associated with DNA repair were the most represented in the upregulated dataset, while the protein import in the mitochondria was the most represented function in the downregulated dataset (Supplementary Figs. 1–2). A merged dataset containing the upregulated and downregulated proteins was submitted to the Ingenuity Pathway Analysis tool (IPA, Qiagen). Surprisingly, the IPA downstream analysis predicted increased cell survival and decreased apoptosis (Supplementary Fig. 3). The IPA upstream analysis revealed that cell survival could be

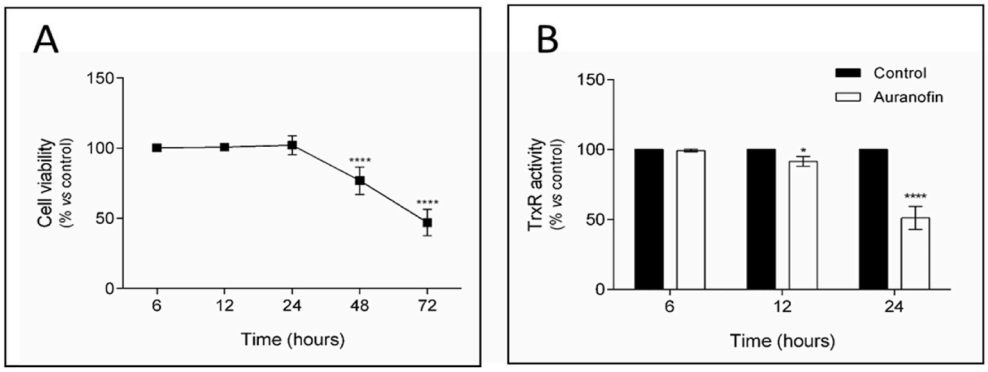

Fig. 1. Fig. 1 (A) Cell viability time course upon auranofin treatment using MTT assay. Values were obtained by measuring the percentage of treated-A2780 viable cells relative to untreated controls after 6, 12, 24, 48, and 72 h of incubation with AF 72 h-exposure IC_{50}-dose. (B) TrxR enzyme inhibition time course assay was performed at 6, 12 and 24 h of treatment using a commercial thioredoxin reductase assay kit (Sigma-Aldrich). All the results are reported as mean ± SD of at least three independent biological experiments analyzed in triplicate. The statistical analysis was carried out by a two-tailed T-test using Graphpad Prism v 6.0 (*$p < 0.05$, ****$p < 0.0001$).

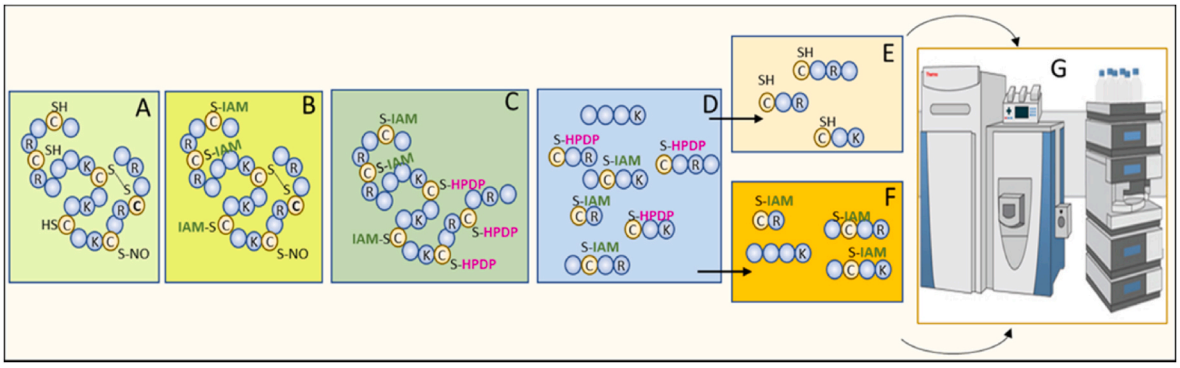

Fig. 2. Workflow of the cysteine redox proteomics workflow. In the step A, reduced thiols (-SH) are alkylated with a high concentration of iodoacetamide as showed in previous studies [41,42]. In the step B, after removing IAM, reversible thiol oxidations are reduced by DTT. In the step C, after DTT removal, the newly generated reduced thiols form a mixed disulfide with biotin-HPDP. In step D, the proteins are trypsin digested and loaded onto a streptavidin resin. In step E, biotin-HPDP labeled peptides are eluted by DTT cleaving the biotin arm. The bound and unbound peptide fractions (panel F) are analyzed by LC-MSMS (panel G) in separate runs.

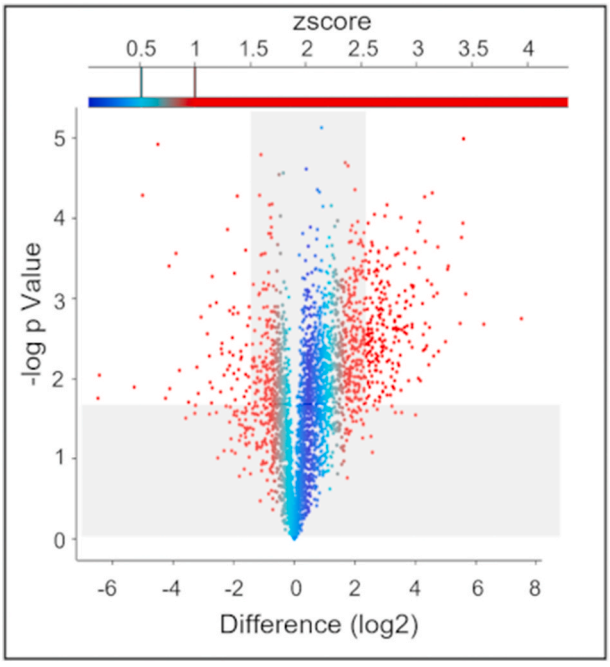

Fig. 3. Volcano plot of the protein expression profiles. Positive values correspond to protein upregulation. Red dots in the white region of the graphic are considered statistically significant fold changes. (For interpretation of the references to color in this figure legend, the reader is referred to the Web version of this article.)

related to the activation of transcription factors associated with the HSPs and DNA damage responses (Supplementary Fig. 4). These results point to the detection of drug adaptation/resistance mechanisms. Interestingly, the upstream analysis predicted Breast Cancer Type 1 Susceptibility Protein (BRCA1) as a possible transcription factor involved in AF-induced DNA repair mechanisms (Supplementary Fig. 4). In agreement with this result, BRCA1 deficiency was already shown to sensitize ovarian cancer cells to AF [31]. Compared to other gold compounds, AF was shown to bind DNA poorly [45], and its deleterious effects were hypothesized to be ROS-mediated [46]. BRCA1 activation could be linked to the defect of DNA synthesis resulting from the inhibition of Ribonucleoside Reductase (RNR) catalytically dependent on Trx. The network analysis of our dataset by IPA revealed the enrichment of a protein network centered on RNR (Fig. 4A). Both RNR1 and RNR2 were upregulated in AF-treated cells, highlighting the response of cells to TrxR1 inhibition. The second top-ranked upregulated network was centered on Caspase 3, proving the pro-apoptotic effects of AF (Fig. 4B). The AF-mediated Caspase 3 activation was also previously observed [11].

The activation of NRF2 transcription factor by AF was reported in the literature [47–49]. The upstream analysis of our proteomic dataset did not reveal the activation of NRF2 by AF. However, we found several upregulated proteins under the NRF2 transcriptional control (TrxR1, SRX, GCLC, GCLM, GSTM2, G6PD, PGD, ME1) consistent with the activation of this well-known transcription factor. The upregulation of HMOX, another well-known NRF2 target was detected in previous AF studies [25,49,50]. In agreement, we measured for HMOX a fold change increase of 2.7 with a p-value of 0.03. However, HMOX is not in the list of upregulated proteins because of the stringent statistic thresholds we have introduced using the Z-score > 1 (HMOX Z-score = 0.8).

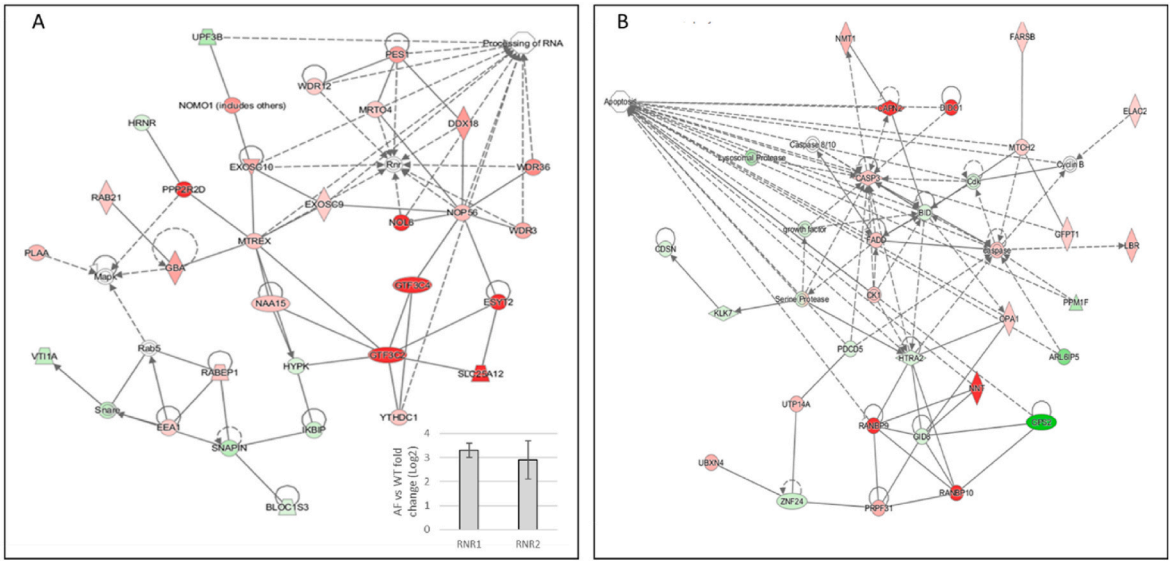

Fig. 4. Enriched protein networks obtained with Ingenuity Pathway Analysis. Performing the network analysis in the Ingenuity framework, Ribonucleoside Reductase (RNR) resulted in being at the center of the network of a cluster of upregulated proteins (panel A). RNR1 and RNR2 resulted upregulated in the Auranofin treated samples as shown in panel A, where the histograms represent the fold change (Log2) of RNRs expression compared to the untreated samples., Caspase 3 resulted to be at the center of the second top-ranked enriched network pointing to the caspase-mediated apoptosis (panel B).

The cysteine redox analysis quantified 3748 reduced and 1015 oxidized Cys residues (Supplementary Tables 2 and 3). To differentiate redox effects from protein level regulation, the oxidized/reduced Cys-containing peptide ratios were normalized by the associated protein expression ratios. Thus, our redox proteomics strategy detects the variation of oxidized/reduced cysteine fraction instead of providing an absolute concentration. Decreased levels of 333 reduced Cys (in 228 proteins) and increased levels of 436 were detected (in 275 proteins) (Fig. 5A). Moreover, 40 oxidized Cys (in 38 proteins) showed decreased levels while 84 (in 69 proteins) increased (Fig. 5A). Peptides containing multiple Cys residues showing different redox states were separately considered (Supplementary Table 4). Altered levels of 18 peptides containing multiple Cys in different redox states were found.

The lists of potentially oxidized Cys residues after AF-treatment (with increased levels of the oxidized form or decreased levels of the reduced form) were submitted to the bioinformatics tool Cpipe. This is a comprehensive computational platform to investigate Cys reactivity and predict their possible functional roles [51]. Chemical-physical features are estimated by probabilistic scores indicating the tendency of Cys residues to exhibit a given feature. We first created a background list of Cpipe chemical-physical parameters for all the cysteines belonging to the proteins detected in our proteomic analysis for which a three-dimensional structure (PDB file) was available (Supplementary Table 5, Fig. 5B). This background list was considered as a reference (control) of the cysteine chemical-physical features at the proteome scale. We found that 9% of the Cys residues in the background list have high scores (>0.75) for the tendency to be post-translationally modified, 7% for the exposition, 14% for the tendency to bind metals, 7% for the

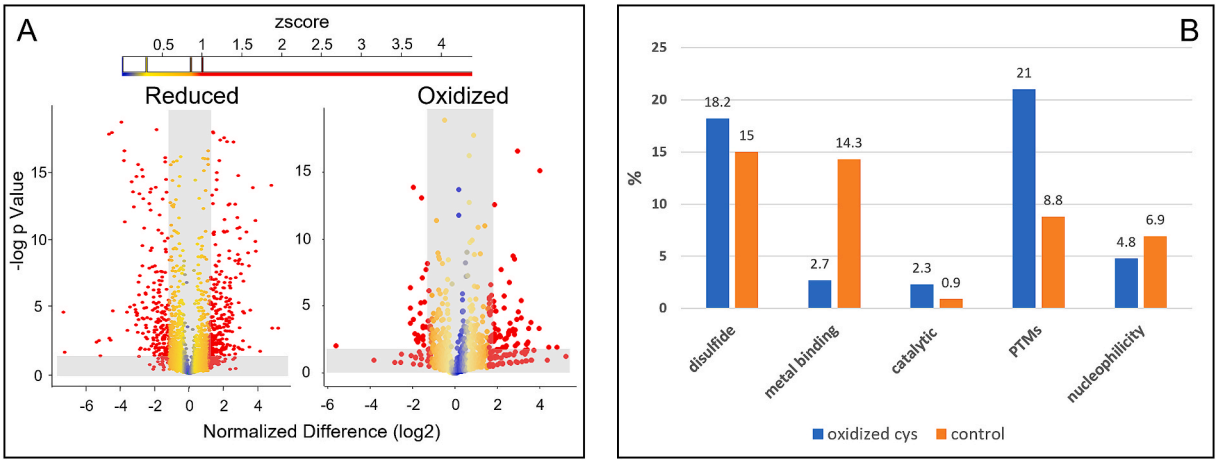

Fig. 5. Volcano plots of the reduced and oxidized Cys fold changes. Fold changes were normalized by protein expression levels. Quantitative proteomics data were obtained from three biological replicates. Panel C: Chemical-physical features of the potential oxidized cysteines from Cpipe analysis. Cpipe calculates a probability score (values between 0 and 1) evaluating the tendency of a Cys residue to exhibit a given chemical-physical feature. We built a background list (control) containing the Cpipe scores for all Cys residues detected in our proteomic analysis (when a PDB file was available). Then, we calculated for the background list and for the oxidized cysteine list the percentage of Cys residues exhibiting a score >0.75 for the tendency to be post-translational modified (PTM), to be exposed (exposition), to bind metals (metal binding), to be nucleophile (energy) and to form disulfide bonds (disulfide). A higher percentage of cysteine residues found with increased oxidized level (in orange) after AF treatment showed a PTM score >0.75 compared to the background list. A lower percentage showed metal-binding scores >0.75. (For interpretation of the references to color in this figure legend, the reader is referred to the Web version of this article.)

nucleophilicity, 1% for the catalytic activity, 15% for forming disulfide bonds. Interestingly the percentage of the Cys residues detected more oxidized with scores >0.75 for the tendency to bind metals (97% of the detected oxidized cysteines showed metal affinity scores<0.5) is lower after the AF treatment than the background list. This result is consistent with the hypothesis that metal ligation could protect thiols from oxidations [52]. Moreover, the percentage of cysteines withe scores >0.75 for PTM (Fig. 5B) is higher. These observations suggest that the observed Cys oxidations are more likely related to the oxidative damage consequent to the AF treatment than to the direct interaction with the metal-based drug.

The list of potentially oxidized Cys was then submitted to the bioinformatics tool DAVID for gene ontology enrichment analysis. The ribosome turned out to be the most affected Kegg's pathway (Supplementary Fig. 5), while oxidative phosphorylation and the response to inorganic substances were the most affected biological functions.

In the light of these observations, we can now propose a global description of AF effects on Trx-GSH pathways and the mitochondria-ER cross-talk.

3.2. The effects of AF on thioredoxin and GSH pathways

TrxR1 was upregulated after AF treatment, in agreement with a previous study [39]. Indeed, protein upregulation was reported to be an excellent readout to detect drug targets [53]. We also detected unaltered normalized levels of catalytic Cys in the reduced form. This is compatible with the biosynthesis of active TrxR1 to counterbalance the effects of AF inhibition. The mitochondrial TrxR2 level was not found altered. Interestingly, we did not detect any change of protein expression in TRXs or PRDXs, while we detected an increased level of sulfiredoxin (SRX) (Fig. 6A) responsible for PRDXs recovery from the sulfinylated form. The fraction of the oxidized form of the SRX catalytic Cys residue (C99) decreased (Fig. 6B) whereas the C99 reduced form and protein fold changes were similar. These results are compatible with the increase of SRX synthesis in the active reduced form. The increase of SRX levels could be an adaptative response to the PRDXs increased activity. The redox-active Cys residues C100 (peroxidatic residue) and C204 (resolving residue) of the mitochondrial peroxiredoxin PRDX5 were found with increased and decreased levels of the reduced forms, respectively. This configuration could be associated with the accumulation of an inactive PRDX5 form with the resolving cysteine hyperoxidized, avoiding the accumulation of the intramolecular disulfide bridge [54]. The levels of Trx1 and Trx2 isoforms with the nucleophilic cysteine reversibly oxidized and the resolving cysteine reduced were found increased.

Other thioredoxin-like proteins were found with altered levels. TXNL1 was highly downregulated in AF-treated cells. The downregulation of TXNL1 was already reported as a factor of resistance to cisplatin in gastric cancer [55]. TXNDC5 was upregulated. TXNDC5 upregulation compensates for the deficiency of Protein Disulfide Isomerase (PDI) activity in the endoplasmic reticulum (ER).

Previous work reported that GSH levels increased in AF-treated A2780 cells [56]. Accordingly, in our study, GCLM and GCLC involved in the GSH synthesis were upregulated in AF-treated cells, while the glutathione synthase showed no significant changes. Therefore, it was hypothesized that GSH participates in gold detoxification. Glutathione transferases (GSTs) are also involved in metal detoxification and drug cell resistance by favoring their conjugation to GSH [57]. The two key chemotherapeutic drugs' detoxification agents [58] GSTT1 and MGST1 were upregulated. As for the thioredoxin pathway, we did not detect significant changes in the expression profiles of glutaredoxins (GLRXs) and glutathione peroxidases (GPXs), while we detected an increased

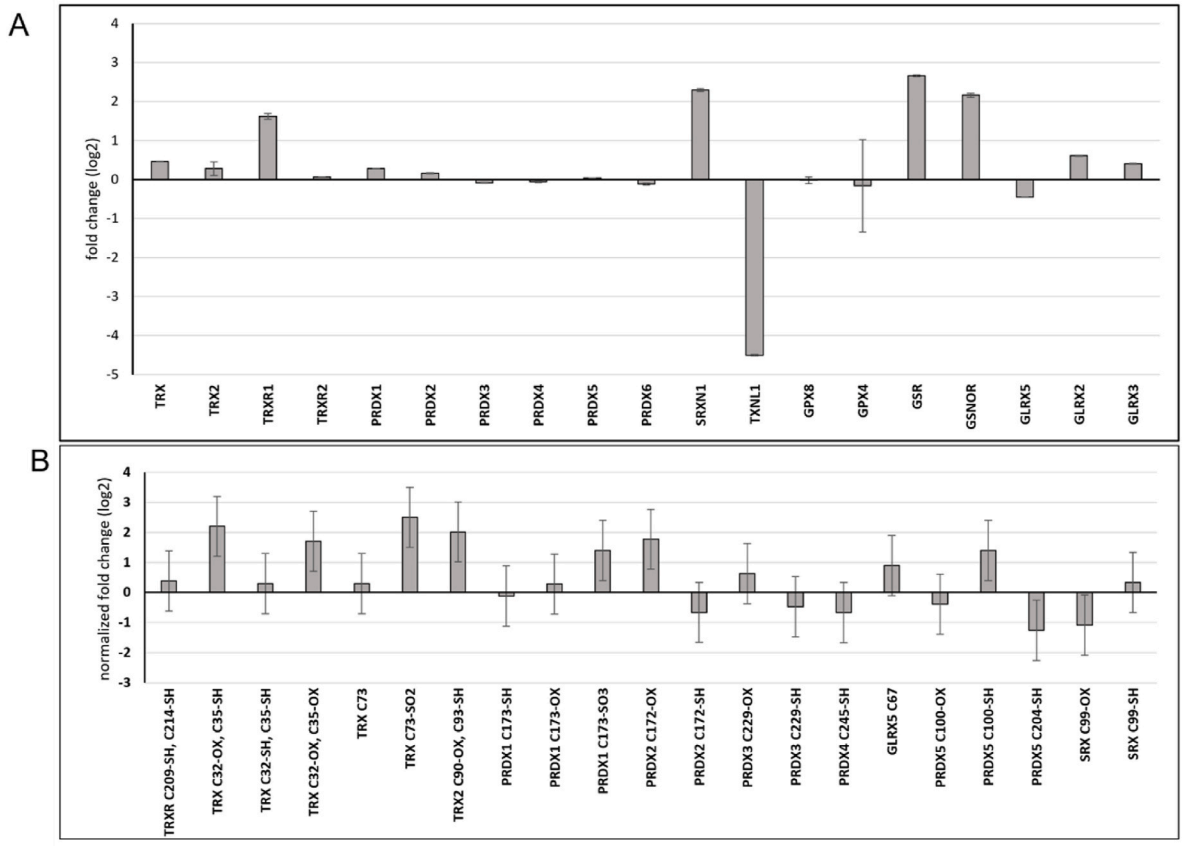

Fig. 6. (A) Fold changes measured for some Trx and GSH pathway proteins. (B) Fold changes normalized by protein expression for some oxidized/reduced cysteines belonging to TRX and GSH pathway proteins.

level of Glutathione Reductase (GSR) that plays a role similar to TrxR in the GSH pathway and of *S*-nitrosoglutathione reductase (GSNOR, also called Alcohol Dehydrogenase 5, ADH5). GSNOR is upregulated by the redox activation of ATM, a key protein in the DNA repair pathway [59], which was experimentally confirmed in our proteomics data.

3.3. AF induced mitochondrial stress: oxidative phosphorylation (OXPHOS)

There is now considerable evidence to support that the main AF-mediated cytotoxic effects are related to the mitochondrial stress impairing OXPHOS [60,61]. Despite this, a global unbiased proteomics approach was still missing. The bioinformatic analysis of our dataset revealed that OXPHOS was one of the affected pathways by cysteine oxidation. Moreover, Kegg's pathway analysis showed that complexes I, III, IV, and V were downregulated (Supplementary Fig. 6). These results were confirmed by Western blot analysis (Fig. 7A). To confirm the impairment of the OXPHOS in AF-treated A2780 cells, we measured the level of oxygen consumption and lactate production (Fig. 7B). The results confirm the impairment of OXPHOS and the switch to glycolytic metabolism. This effect, also known as the Warburg effect, is considered as an antiapoptotic event that could alter drug efficacy [62].

Under stress conditions, OXPHOS activity is decreased with cytoprotective effects by the mitochondrial chaperon Tumor Necrosis Factor Receptor-Associated Protein 1 (TRAP1) [63]. According to previous reports, the *S*-nitrosylation of TRAP1 C501 decreases TRAP1 protective activity against different drugs targeting mitochondria [64] and also decreases ATPase activity [65]. Our redox proteomics study detected the TRAP1 C501 reduced form decreased in AF-treated A2780 cells (Supplementary Table 6). This result raised the question about the role of C501 on AF toxicity. Indeed, when exposed to 0.7 μM AF, A2780 cell line expressing the C501S mutant of TRAP1 exhibited reduced cell death and apoptosis compared to the control (untreated) (Fig. 7C–D), suggesting that C501 oxidation could be a mediator of AF toxicity.

Although this experiment does not fully elucidate the functional role of C501 oxidation observed by redox proteomics, it demonstrates that C501 modulates the AF toxicity and point mutations on this residue can alter the drug efficiency.

3.4. AF induced mitochondrial stress: effects on the mitochondrial protein import machinery

The import of newly synthesized proteins into the mitochondria matrix is a Cys redox-mediated mechanism involving the Trans Outer Mitochondrial Membrane proteins (TOMMs) at the interface between the cytoplasm and mitochondria. A Cys redox relay system is based on the oxidoreductase GFER (also known as ERV1) and CHCHD4 (also known as MIA40) and the Trans Inner Mitochondrial Membrane proteins (TIMMs) in the Inner Membrane Space (IMS) (Fig. 7E). Considering the protein expression levels, we detected a decrease of 5 TIMMs and CHCHD4 and unaltered levels of GFER and the TOMMs (Fig. 7E and Supplementary Table 6). The complexes TIMM8/TIMM13 and TIMM9/TIMM10 and CHCHD4 participate in the IMS protein folding and are downregulated after AF treatment. The residue C87 in CHCHD4, essential for the protein import in the mitochondria, was found less oxidized. C87 is linked with C74 by a disulfide bridge in the CHCHD4 active oxidized form [66]. GFER that oxidizes CHCHD4 by a cysteine redox relay showed decreased level of the oxidized C95, which is involved in the interchain disulfide bond with C204 to form the active homodimer. GFER/CHCHD4 redox system is connected to OXPHOS. Indeed, blocking the Cytochrome-c oxidase (Complex IV) activity leads to the accumulation of reduced CHCHD4 [67]. As mentioned above, we detected 4 downregulated subunits of Complex IV within a global alteration of OXPHOS induced by AF. Thus, the impairment of the

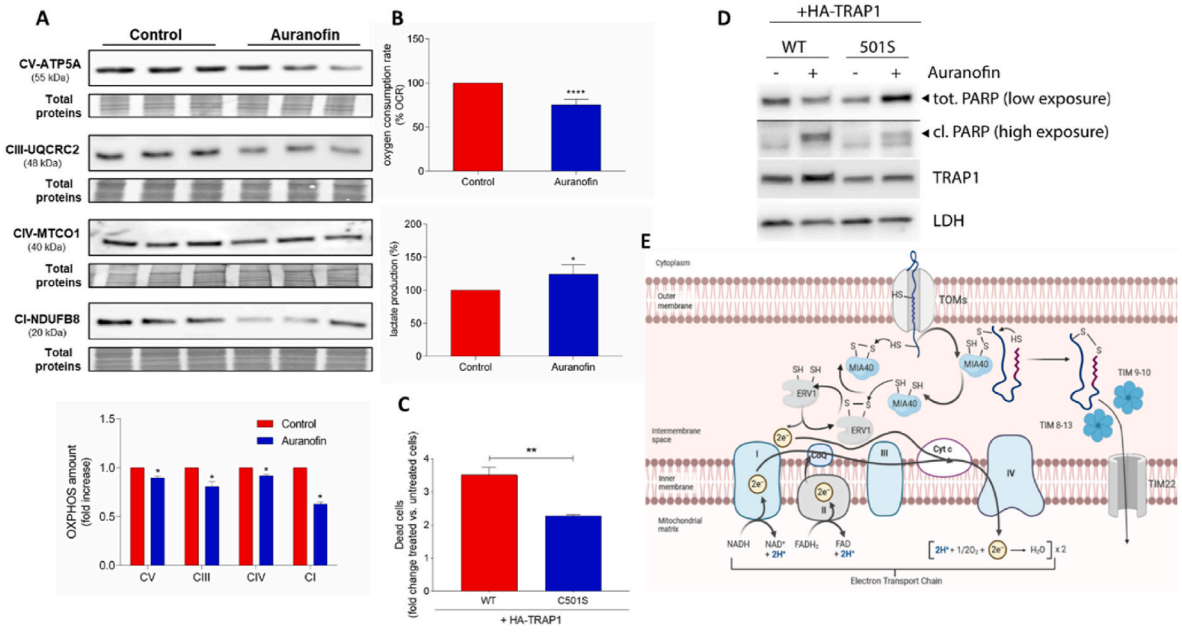

Fig. 7. (A) Western blot analysis of some OXPHOS subunits. Representative Immunoblots are shown together with the corresponding Coomassie-stained PVDF membranes. Histogram reports normalized mean relative-integrated-density ± SD values of the OXPHOS bands. The statistical analysis was carried out using one-way ANOVA test followed by Tuckey's multiple comparisons test using Graphpad Prismv v.6.0 (*$p < 0.05$). (B) Oxygen consumption rate measured by Clark's electrode and lactate production. Histograms report the mean values ± SD of at least three independent experiments. The statistical analysis was carried out by a two-tailed T-test using Graphpad Prism v 6.0 (*$p < 0.05$, ****$p < 0.0001$). (C) Cell death analysis of A2780 cells transfected with WT or C501S HA-TRAP1. Dead cells were measured by flow cytometry evaluating the percentage of cells in Sub-G1 population following Propidium Iodide staining. The histogram shows fold change (AF treated versus untreated cells) in the number of dead cells as mean ± s.e.m. of three independent experiments. Significance is **, $p < 0,01$ ($p=0,0056$) by two-tailed Student's T test. (D) PARP1 cleavage was evaluated in WT and C501S A2780 cells by Western blot analysis with anti-PARP1, anti-TRAP1 and anti-LDH antibodies (E) Schematic representation of IMS folding machinery. Blue icons represent downregulated proteins in AF-treated cells. (For interpretation of the references to color in this figure legend, the reader is referred to the Web version of this article.)

electron transport chain can also have deleterious effects on the mitochondrial protein import machinery. Accordingly, the IMS zinc-metalloprotease YML1 was upregulated in AF treated cells. YML1 is responsible for the degradation of the unfolded CHCHD4 targets, such as TIMM9/TIMM10 and NDUFA8 [68] which, accordingly, were found downregulated in AF treated cells.

Another essential IMS protein up-levelled in reduced Cys fraction is the Cytochrome-c heme lyase (HCCS). HCCS mediates the assembly of the heme group with the apo Cytochrome-c via disulfide bond exchange [69]. In our data, residues C176 and C178 (C–P–C motif) were more reduced in AF-treated cells. No study about the human heme-apo Cytochrome-c assembly mechanisms is available. However, in yeast, it was shown that the HCCS C–P-X sequence motif could interact with heme [70]. Thus, Cys residues in C176– C178 could be potential actors of the Cytochrome-c maturation.

Heme assembling is realized in the mitochondria matrix, and we detected perturbations in mitochondrial iron metabolism proteins after AF treatment. For instance, the Fe–S cluster assembly proteins ISCA2 and Ferredoxin 2 were down-levelled (Supplementary Table 6).

3.5. AF induced mitochondrial stress: the effects on the mitochondrial membrane permeability transition pore (mPTP)

A previous study reported that AF induces the mitochondrial membrane permeability transition [71]. Voltage-Dependent Anion Channel proteins (VDAC) play an essential role in the mPTP opening. VDACs are also involved in the Cytochrome-c release mediated by Ca^{2+} uptake and the BAX-BCL2 ratio [71]. In our proteomics dataset, we found higher levels of VDAC3 in AF-treated cells. Similar independent results were found after treatment with arsenic trioxide, an alternative TrxR1 inhibitor [72].

Peptidyl-prolyl *cis*-trans isomerase F, also known as Cyclophilin D, is involved in the regulation of mPTP opening. We found increased levels of reduced Cys residue Cyclophilin D C157 in AF-treated cells. Even though no functional roles are reported in the literature, Cpipe analysis suggested that residue C157 is the most reactive Cyclophilin D Cys residue and can form an intramolecular disulfide bond with C62 (Supplementary Fig. 7); in addition it can be S-nitrosylated in mice. Despite the reduced C157 showed a 2.5-fold increase in the AF samples, we estimated from our redox proteomics dataset that oxidized C157 residue still has a high site occupancy (as defined by Olsen et al., [73]): 96% in the control cells and 91% in AF-treated cells. Since Cyclophilin D is involved in mPTP opening by cysteine redox mechanisms with the less reactive C203 [74], it is expected that C157 could also be involved, even if this hypothesis needs to be further verified by a targeted study. The mitochondrial membrane Ca^{2+} carrier SLC25A13 is part of the mitochondrial permeability transition pore complex with VDAC and Cyclophilin D [75] and was also upregulated upon AF treatment.

Dynamins and dynamins-like proteins participate in the mitochondrial membrane stability, remodeling and Cytochrome-c release into the cytoplasm [76]. We observed increased levels of Dynamin-related protein 1 (DNRP1), Dynamin 2 and Dynamin-like protein OPA1.

The AF-mediated increase of mitochondrial membrane permeability is thus a macroscopic effect consistent with the molecular effects described in our proteomics data.

3.6. AF induced ER stress

It was recently shown that a robust TxrR/Trx pathway is necessary to correctly form native disulfides in the ER [77,78]. However, the electron transfer mechanisms across the ER membrane are not characterized yet. The ER transmembrane oxidoreductase TMX1 has a redox-active motif C56-XX-C59 in the ER lumen and C205-X-C207 in the cytosol (quantitative data discussed in this paragraph are summed up in Supplementary Table 6). It is involved in different thiol-dependent mechanisms, such as the reductive process of ER-associated degradation (ERAD) of misfolded proteins [79], and in the regulation of ER Ca^{2+} levels, regulating the Sarco-Endoplasmic Reticulum Calcium ATPase 2 (SERCA2) [80]. Interestingly, according to STRING and Biogrid bioinformatic predictions (Supplementary Fig. 8), TMX1 interacts with Trx, making it a potential candidate for the cross-talk between the cytosolic TrxR/Trx pathway and ER. Furthermore, it was shown that the redox-active ER lumen Cys residues C56 and C59 of TMX1 are mainly in the reduced form [81]. Unfortunately, the measurement of the redox state of C56-XX-C59 and C205-X-C207 by MS-based proteomics is inconclusive because trypsin digestion generates large peptides around these motifs (>5 KDa). However, by inhibiting TrxR with AF, the level of the reduced state of TMX1 C106, one of the four ER lumen Cys residues, decreased. Moreover, as an indirect readout, we can monitor the oxidation state of the resolving Cys residues of the Vitamin K epoxide reductase family (VKORs) under the redox control of TMX1 C56/C59 [82]. Interestingly, we detected an increased oxidation level of the VKORC1L1 resolving cysteine C50. These results are consistent with a decreased TMX1 reductase activity.

There is considerable evidence supporting the cross-talk between ER and mitochondria in response to apoptotic stimuli [83]. The ER Unfolded Protein Response (UPR) was one of the enriched biological functions in AF-treated cells. Moreover, as shown in Fig. 8, many proteins belonging to the ERAD were upregulated, including those involved in the ubiquitination process. The increased levels of protein ubiquitination were already reported as an AF effect in HCT116 colon carcinoma cells [37]. In agreement with our proteomics data, we confirmed by Western blot that AF increases the ubiquitination rate in A2780 ovarian cancer cells (Fig. 9A). The increased expression level of ERAD is associated with the accumulation of misfolded proteins in the ER. Accordingly, we detected an increased level of ER chaperones HSP70s (HSPA2, HSPA4, HSPA4L, HSPA13) HSP90 (HSP90AB1) and of proteins involved in the deglycosylation-glycosylation process (UGGT1, GANAB).

The ER-Oxidoreductin 1 (ERO1) forms, with the Protein Disulfide Isomerases (PDIs), the thiol redox relay system for the formation and isomerization of disulfide bridges. ERO1 is induced by UPR [84], and it transfers its oxidizing equivalent to PDIs. The level of ERO1 increased in AF-treated cells (confirmed by Western blot, Fig. 9C), while PDIs levels were unaltered. Considering the thiol redox status, the reduced states of Cys residues ERO1 C208, PDIA3/ERP57 C57, and C60 were more abundant. However, according to Cpipe, these cysteine residues should be engaged in disulfide bridges. Simultaneously, the oxidized states of PDIA1 C343, TXNDC5 C247, and TXNDC5 C254 were less abundant. The increased abundance of reduced states and the decreased abundance of oxidized states are consistent with a lower reduction potential of the ER. In agreement with this observation, the abundance of reduced states of PDIA3/ERP57 catalytic Cys residues increased. PDIA3/ERP57 modulates SERCA2 (ATP2A2) that mediates Ca^{2+} uptake in the ER. It binds to SERCA2 which stabilize the oxidized form that is less active. When the Ca^{2+} concentration drops, the ER is more reducing [85], PDIA3/ERP57 dissociates from SERCA2, and the Ca^{2+}channel opens for the intake [86]. We detected increased levels of SERCA2. Interestingly, the ER disulfide reductase DNAJC10 which reduces the SERCA2 luminal disulfide bond and opens the channel [87] was also upregulated. Altogether, this data points to an activation of the pump to restore an advanced state of Ca^{2+} depletion.

ERO1 upregulation potentiates the Ca^{2+} release from ER, mediated by inositol 1,4,5-trisphosphate receptor (IP3R) [88]. The activation of Ca^{2+} signaling agrees with the increased level of Calpain2 (CAPN2) detected in AF-treated cells and, globally, with ER-mediated permeabilization of the mitochondrial membrane discussed above. Calpains and Ca^{2+} regulate the BAX/BAK activation and migration to the mitochondrial membrane [89,90]. Western blots targeting the levels of BAX and BCL2 proteins demonstrate an increased BAX/BCL2 ratio compared to the control (Fig. 9B). BAX forms a complex with BID to migrate to the mitochondrial membrane [91] as an ER stress downstream effect mediated by the Caspase 8 [92]. The increased FAS-associated death

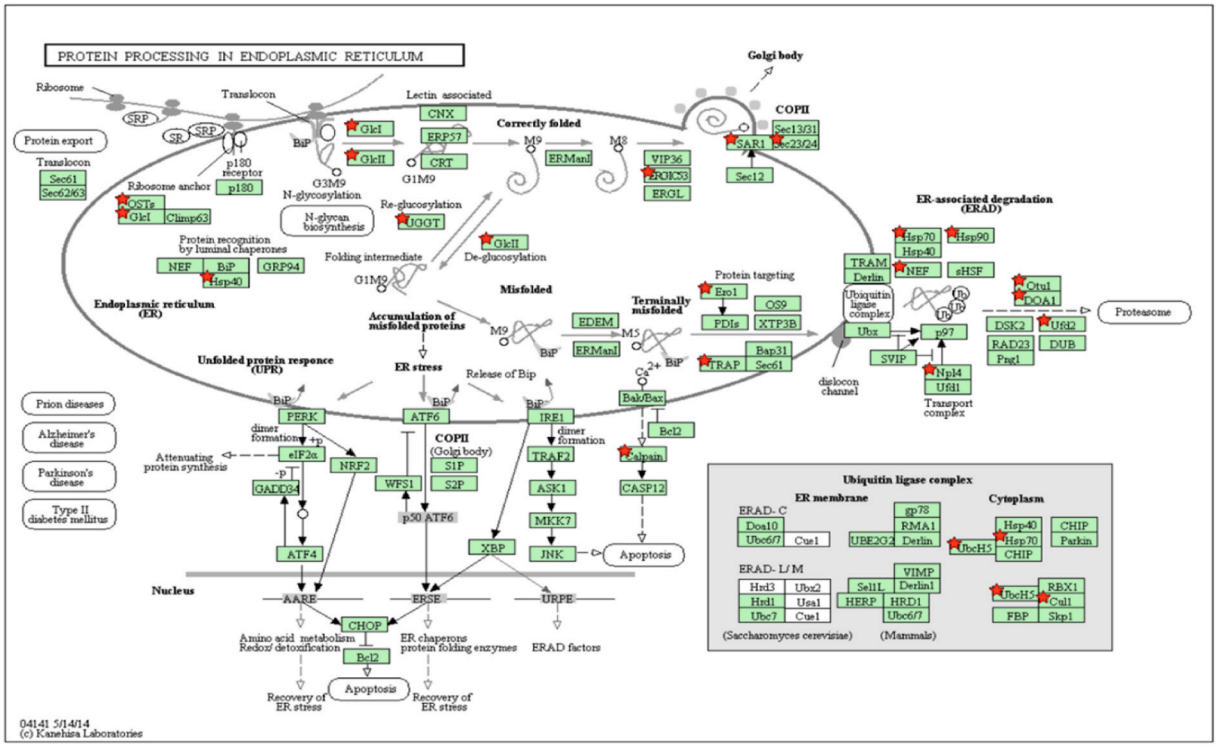

Fig. 8. Kegg's pathway representation of the Protein Processing in ER pathway. The list of upregulated protein was submitted to the bionformatics tool DAVID. Protein Processing in ER was one of the enriched Kegg's pathways (Benjamini corrected p-value = 0.01). The proteins highlighted by a red star were found upregulated. (For interpretation of the references to color in this figure legend, the reader is referred to the Web version of this article.)

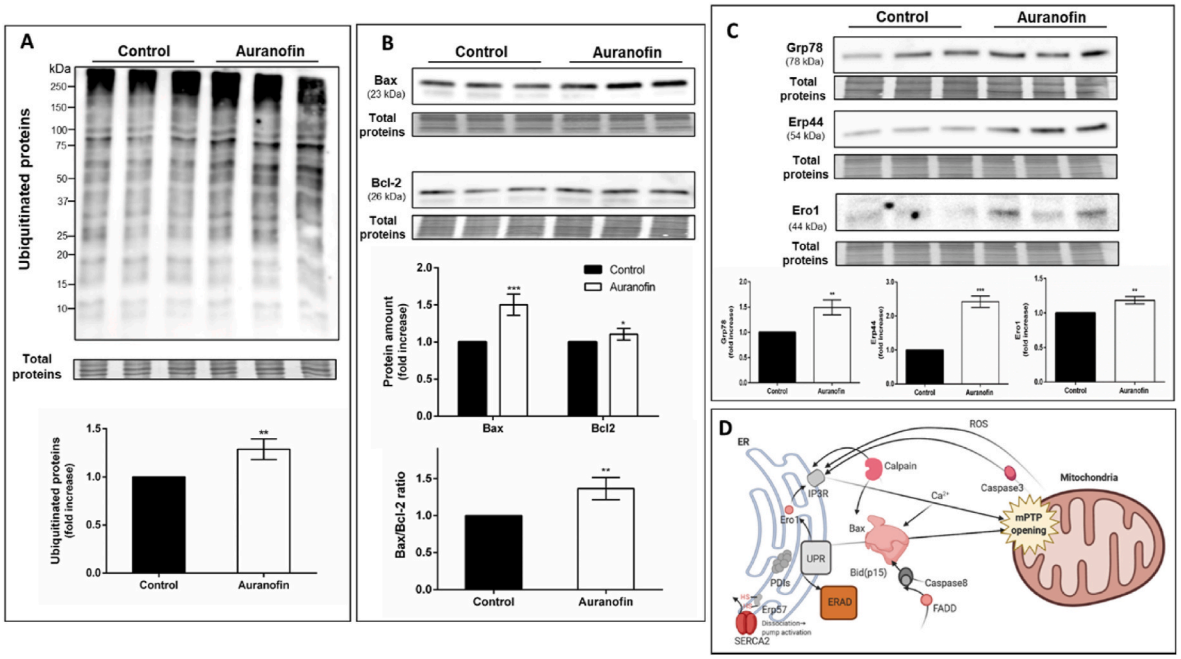

Fig. 9. (A). Ubiquitinated protein level. Representative Immunoblots are shown together with the corresponding Coomassie-stained PVDF membranes. Histogram reports normalized mean relative-integrated-density ± SD values of the ubiquitinated protein bands. The statistical analysis was carried out by a two-tailed T-test using Graphpad Prism v 6.0. (*p < 0.05, **p < 0.01, ***p < 0.001, ****p < 0.0001). (B) Bax and Bcl-2 protein amount. Representative Immunoblots are shown together with the corresponding Coomassie-stained PVDF membranes. (C) Immunoblots of GRP78, ERp44 and ERO1 in control and AF treated A2780 cells. (D) Schematic representation of ER/mitochondria cross-talk highlighted by our proteomics results. Red icons represent up-regulated proteins.

domain protein (FADD) levels correlate with an ER stress-mediated Caspase 8 activation. These results suggest that AF induces severe ER stress and ER-mediated mitochondrial membrane permeabilization at IC_{50} doses in A2780 cells (Fig. 9D). The detected downregulation of Mesencephalic astrocyte-derived neurotrophic factor (MANF) further indicates severe ER stress. Indeed, MANF is target of the IRE1-dependent

decay (RIDD) that degrades the mRNA of ER-stress response proteins under prolonged ER stress [93]. We finally performed Western blots targeting the levels of GRP78 (BiP) and ERP44, two ER stress markers not quantified by mass spectrometry: they were found upregulated in AF-treated samples (Fig. 9C).

4. Conclusions

This thiol redox proteomics study provides a global overview of the already known mechanisms underlying AF cytotoxicity. It provides new data-driven hypotheses for future studies. Besides helping to understand the role of AF in cancer therapy, we think that TrxR1 inhibition by thiol redox proteomics is also invaluable for fundamental thiol biology studies. At the best of our knowledge, only very few studies have been realized so far from this point of view, despite AF affecting mainly the thiol redox homeostasis. Our redox proteomics workflow complements the study based on a redox ICAT (Isotope Coded Affinity Tag) approach performed by Go Y.M et al. [38]. In a single analysis, we simultaneously monitored the alteration of protein expression profiles and the cysteine oxidations. This analytical strategy leads to better modeling the system under analysis and better understanding the cysteine redox events. For example, in AF-treated cells, the oxidized fraction of the SRX catalytic cysteine is down-leveled, which is at first glance in contradiction with undergoing oxidative stress. However, with the simultaneous detection of SRX overexpression, our data suggest the enhanced biosynthesis of the active reduced form, which consequently decreases the relative fraction of inactive oxidized catalytic cysteine. This conclusion underlines the importance of the simultaneous monitoring of protein level and individual Cys redox event extent. Globally, compared to previous proteomics studies [33–39], our results offer a comprehensive vision of the biochemical aspects of AF cytotoxicity covering a larger number of molecular pathways.

Ovarian cancer cells are sensitive to AF treatment. Notably, the therapeutic efficacy of AF is now in phase 2 evaluation in patients affected by serous ovarian tumors (ClinicalTrials.gov Identifier: NCT03456700). Landini et al. characterized an AF-resistant ovarian cancer cell line and reported that the alteration of gold uptake mediated by the organic cation/anion efflux system could be one of the mechanisms underlying the drug resistance [94]. Besides the expected cell death mechanisms involving the canonical intrinsic apoptosis pathway, the present study revealed some interesting details of the ovarian cancer cell adaptative response to AF treatment. The most significant alterations concerned GSH, BRCA1, TRAP1 and ER stress. Additional details on these biomolecules and their respective importance in cancer biology and drug mechanisms are given below.

4.1. GSH

Interestingly, in A2780 cells sensitive to AF, we found increased levels of glutathione transferases involved in metal detoxifications by the conjugation of GSH with the electrophilic compounds. Additional studies are necessary to test if GSH is the principal actor of the intracellular gold detoxification. These observations are consistent with other studies showing that cancer cells resistant to AF were sensitized to the treatment if exposed to the GSH synthesis inhibitor Buthionine Sulfoximine (BSO) [95,96]. Authors attributed such sensitization to an additional decrease of the ROS scavenging capacity in cells lacking GSH while an alternative explanation could be the decreased gold efflux from cells.

4.2. BRCA1

We found increased levels of BRCA1 downstream proteins involved in DNA repair. This could be associated with the alteration of Trx-dependent RNR activity. Ovarian cancer cells lacking BRCA1 are more sensitive to AF treatment [31]. It is not uncommon that oncosuppressors can act as oncogenes after the malignant cell transformation. In this case, the DNA repair and antioxidant features of BRCA1 can induce cancer cell survival and drug resistance. It was indeed reported that the most diffused ovarian cancer subtype (High-Grade Serous) presents BRCA1 mutations affecting its functions [97]. This confirms that such ovarian cancer is an excellent candidate for AF treatment.

4.3. TRAP1

The increase of the oxidized state of TRAP1 C501 led us to investigate its role in response to AF treatment. Our data suggested that C501 oxidation is a mediator of AF toxicity, and we found that C501S mutation decreased the cell sensitivity to AF treatment. As previously reported, TRAP1 C501 *S*-nitrosylation impacts its protein expression levels and ATPase activity, both important for TRAP1 role in regulating the Warburg effect and sensitivity to drugs [63,64,98,99]. Here, the observed decreased sensitivity of the TRAP1 C501S mutant to AF agrees with the effects of C501 *S*-nitrosylation shown in previous studies. However, C501 *S*-nitrosylation is favored by low GSNOR levels [64] which, conversely, we detected increased in AF-treated cells. Moreover, C501 *S*-nitrosylation has been associated with TRAP1 degradation [64], while no significant changes in TRAP1 relative abundance were detected in our study. These results suggest that the increase of an alternative cysteine reversible oxidation was observed in AF-treated cells. Further studies are necessary to describe the chemical structures of oxidized C501 residue and their effects on AF toxicity.

4.4. ER stress

TrxRs inhibition is undoubtedly an important therapeutic target. However, it is also exploited in fundamental thiol biology studies to understand the molecular mechanisms of thiol signaling. Previous studies revealed that AF could induce ER stress and mitochondrial dysfunctions by classical biochemistry approaches [100,101]. Our redox proteomics approach confirmed these alterations and provided mechanistic details. We highlighted the cross-talk between ER and mitochondria with the alterations of the IMS redox folding machinery, the ERAD activation, and the thiol alterations in PDIA3/ERP57 related to the Ca^{2+} release from ER.

Our data concerning the ER stress induced by AF lead to questions and hypotheses needing further dedicated studies. More precisely, the origin of the increased thiol reduction of this compartment should be explored. Is it linked to the Ca^{2+} depletion or an alteration of the GSH/GSSG ratio could take place? Since ER contains 7 selenoproteins, does AF target the ER proteins and increase the GSH influx in this compartment depleting gold? What is the origin of ER stress? Does it result from the decreased oxidizing power or is there a link between Trx pathway and the ER?

In conclusion, this comprehensive and unbiased redox proteomics study allowed us to generate new data-driven hypotheses concerning the possible mechanisms of the AF effect and the associated thiol redox signaling. In addition, it provided molecular information about some relevant processes concerning cell response to gold exposition (that deserve additional studies). In any case, the highlighted processes further suggest that the mechanism of the cytotoxic action of AF is multifactorial, primarily affecting the redox metabolism and the mitochondrial functions and ultimately resulting in severe ER stress.

Acknowledgments

We want to thank Dr. Aeid Igbaria (Ben-Gurion University of the Negev, Israel) and Dr. Agnes Delaunay-Moisan (French Alternative Energies and Atomic Energy Commission, CEA Saclay) for the stimulating discussions concerning the results of this study. Inanc Soylu (Akdeniz University, Antalya, Turkey) for his help with Cpipe software.

This work was supported by the ANR_AAP2019G project ERRED2 n°

197161 and SESAME 2018 - Proteomics@PSL EX039194 KBVU Grant R146-A9414; R231-A13855 and Associazione Italiana per la Ricerca sul Cancro (AIRC) Grant IG20719. LC-MS equipment was supported by SESAME 2018 grant of the Conseil Régional d'Ile-de-France. XL received a Higher Education Learning fellowship from the Erasmus + European program. FF was supported by an "AIRC fellowship for Italy" grant.

Appendix A. Supplementary data

Supplementary data to this article can be found online at https://doi.org/10.1016/j.redox.2022.102294.

References

[1] A.E. Finkelstein, D.T. Walz, V. Batista, M. Mizraji, F. Roisman, A. Misher, Auranofin. New oral gold compound for treatment of rheumatoid arthritis, Ann. Rheum. Dis. 35 (3) (1976) 251–257, https://doi.org/10.1136/ard.35.3.251.

[2] G.C. Bernhard, Auranofin therapy in rheumatoid arthritis, J. Lab. Clin. Med. 100 (2) (1982) 167–177.

[3] B. Chirullo, R. Sgarbanti, D. Limongi, I.L. Shytaj, D. Alvarez, B. Das, A. Boe, S. DaFonseca, N. Chomont, L. Liotta, E. III Petricoin, S. Norelli, E. Pelosi, E. Garaci, A. Savarino, A.T. Palamara, A candidate anti-HIV reservoir compound, auranofin, exerts a selective 'anti-memory' effect by exploiting the baseline oxidative status of lymphocytes, Cell Death Dis 4 (12) (2013) e944, https://doi.org/10.1038/cddis.2013.473.

[4] C.A. Bulman, C.M. Bidlow, S. Lustigman, F. Cho-Ngwa, D. Williams, A. Alberto, J. Rascón, N. Tricoche, M. Samje, A. Bell, B. Suzuki, K.C. Lim, N. Supakorndej, P. Supakorndej, A.R. Wolfe, G.M. Knudsen, S. Chen, C. Wilson, K.-H. Ang, M. Arkin, J. Gut, C. Franklin, C. Marcellino, J.H. McKerrow, A. Debnath, J. A. Sakanari, Repurposing auranofin as a lead candidate for treatment of lymphatic filariasis and onchocerciasis, PLoS Neglected Trop. Dis. 9 (2) (2015), e0003534, https://doi.org/10.1371/journal.pntd.0003534.

[5] N.P. Wiederhold, T.F. Patterson, A. Srinivasan, A.K. Chaturvedi, A.W. Fothergill, F.L. Wormley, A.K. Ramasubramanian, J.L. Lopez-Ribot, Repurposing auranofin as an antifungal: in vitro activity against a variety of medically important fungi, Virulence 8 (2) (2017) 138–142, https://doi.org/10.1080/21505594.2016.1196301.

[6] M.I. Cassetta, T. Marzo, S. Fallani, A. Novelli, L. Messori, Drug repositioning: auranofin as a prospective antimicrobial agent for the treatment of severe staphylococcal infections, Biometals 27 (4) (2014) 787–791, https://doi.org/10.1007/s10534-014-9743-6.

[7] J.M. Madeira, C.J. Renschler, B. Mueller, S. Hashioka, D.L. Gibson, A. Klegeris, Novel protective properties of auranofin: inhibition of human astrocyte cytotoxic secretions and direct neuroprotection, Life Sci 92 (22) (2013) 1072–1080, https://doi.org/10.1016/j.lfs.2013.04.005.

[8] C.K. Mirabelli, R.K. Johnson, C.M. Sung, L. Faucette, K. Muirhead, S.T. Crooke, Evaluation of the in vivo antitumor activity and in vitro cytotoxic properties of auranofin, a coordinated gold compound, in murine tumor models, Cancer Res 45 (1) (1985) 32–39.

[9] T. Onodera, I. Momose, M. Kawada, Potential anticancer activity of auranofin, Chem. Pharm. Bull. (Tokyo) 67 (3) (2019) 186–191, https://doi.org/10.1248/cpb.c18-00767.

[10] C. Marzano, V. Gandin, A. Folda, G. Scutari, A. Bindoli, M.P. Rigobello, Inhibition of thioredoxin reductase by auranofin induces apoptosis in cisplatin-resistant human ovarian cancer cells, Free Radic. Biol. Med. 42 (6) (2007) 872–881, https://doi.org/10.1016/j.freeradbiomed.2006.12.021.

[11] T. Marzo, L. Massai, A. Pratesi, M. Stefanini, D. Cirri, F. Magherini, M. Becatti, I. Landini, S. Nobili, E. Mini, O. Crociani, A. Arcangeli, S. Pillozzi, T. Gamberi, L. Messori, Replacement of the Thiosugar of auranofin with Iodide enhances the anticancer potency in a mouse model of ovarian cancer, ACS Med. Chem. Lett. 10 (4) (2019) 656–660, https://doi.org/10.1021/acsmedchemlett.9b00007.

[12] Z.Y. Pessetto, S.J. Weir, G. Sethi, M.A. Broward, A.K. Godwin, Drug repurposing for gastrointestinal stromal tumor, Mol. Cancer Therapeut. 12 (7) (2013) 1299–1309, https://doi.org/10.1158/1535-7163.MCT-12-0968.

[13] W. Fiskus, N. Saba, M. Shen, M. Ghias, J. Liu, S.D. Gupta, L. Chauhan, R. Rao, S. Gunewardena, K. Schorno, C.P. Austin, K. Maddocks, J. Byrd, A. Melnick, P. Huang, A. Wiestner, K.N. Bhalla, Auranofin induces lethal oxidative and endoplasmic reticulum stress and exerts potent preclinical activity against chronic lymphocytic leukemia, Cancer Res 74 (9) (2014) 2520–2532, https://doi.org/10.1158/0008-5472.CAN-13-2033.

[14] C. Liu, Z. Liu, M. Li, X. Li, Y.-S. Wong, S.-M. Ngai, W. Zheng, Y. Zhang, T. Chen, Enhancement of auranofin-induced apoptosis in MCF-7 human breast cells by selenocystine, a synergistic inhibitor of thioredoxin reductase, PLoS One 8 (1) (2013), e53945, https://doi.org/10.1371/journal.pone.0053945.

[15] G.-X. Hou, P.-P. Liu, S. Zhang, M. Yang, J. Liao, J. Yang, Y. Hu, W.-Q. Jiang, S. Wen, P. Huang, Elimination of stem-like cancer cell side-population by auranofin through modulation of ROS and glycolysis, Cell Death Dis 9 (2) (2018) 89, https://doi.org/10.1038/s41419-017-0159-4.

[16] M.V. Rios Perez, D. Roife, B.B. Dai, Y. Kang, X. Li, M. Pratt, J.B. Fleming, Auranofin to prevent progression of pancreatic ductal adenocarcinoma, J. Clin. Orthod. 34 (4_suppl) (2016) 236, https://doi.org/10.1200/jco.2016.34.4_suppl.236, 236.

[17] I. Romero-Canelón, P.J. Sadler, Next-generation metal anticancer complexes: multitargeting via redox modulation, Inorg. Chem. 52 (21) (2013) 12276–12291, https://doi.org/10.1021/ic400835n.

[18] A. Casini, L. Messori, Molecular mechanisms and proposed targets for selected anticancer gold compounds, Curr. Top. Med. Chem. 11 (21) (2011) 2647–2660, https://doi.org/10.2174/156802611798040732.

[19] T. Marzo, D. Cirri, C. Gabbiani, T. Gamberi, F. Magherini, A. Pratesi, A. Guerri, T. Biver, F. Binacchi, M. Stefanini, A. Arcangeli, L. Messori, Auranofin, Et3PAuCl, and Et3PAuI are highly cytotoxic on colorectal cancer cells: a chemical and biological study, ACS Med. Chem. Lett. 8 (10) (2017) 997–1001, https://doi.org/10.1021/acsmedchemlett.7b00162.

[20] F.D. Sarra, B. Fresch, R. Bini, G. Saielli, A. Bagno, Reactivity of auranofin with selenols and thiols – implications for the anticancer activity of gold(I) compounds, Eur. J. Inorg. Chem. 2013 (15) (2013) 2718–2727, https://doi.org/10.1002/ejic.201300058.

[21] I. Tolbatov, D. Cirri, L. Marchetti, A. Marrone, C. Coletti, N. Re, D. La Mendola, L. Messori, T. Marzo, C. Gabbiani, A. Pratesi, Mechanistic insights into the anticancer properties of the auranofin analog Au(PEt3)I: a theoretical and experimental study, Front. Chem. 8 (2020), https://doi.org/10.3389/fchem.2020.00812.

[22] V. Gandin, A.P. Fernandes, M.P. Rigobello, B. Dani, F. Sorrentino, F. Tisato, M. Björnstedt, A. Bindoli, A. Sturaro, R. Rella, C. Marzano, Cancer cell death induced by phosphine gold(I) compounds targeting thioredoxin reductase, Biochem. Pharmacol. 79 (2) (2010) 90–101, https://doi.org/10.1016/j.bcp.2009.07.023.

[23] O. Rackham, A.-M.J. Shearwood, R. Thyer, E. McNamara, S.M.K. Davies, B. A. Callus, A. Miranda-Vizuete, S.J. Berners-Price, Q. Cheng, E.S.J. Arnér, A. Filipovska, Substrate and inhibitor specificities differ between human cytosolic and mitochondrial thioredoxin reductases: implications for development of specific inhibitors, Free Radic. Biol. Med. 50 (6) (2011) 689–699, https://doi.org/10.1016/j.freeradbiomed.2010.12.015.

[24] M.P. Rigobello, G. Scutari, R. Boscolo, A. Bindoli, Induction of mitochondrial permeability transition by auranofin, a gold(I)-Phosphine derivative, Br. J. Pharmacol. 136 (8) (2002) 1162–1168, https://doi.org/10.1038/sj.bjp.0704823.

[25] X. Zhang, K. Selvaraju, A.A. Saei, P. D'Arcy, R.A. Zubarev, E.S. Arnér, S. Linder, Repurposing of auranofin: thioredoxin reductase remains a primary target of the drug, Biochimie 162 (2019) 46–54, https://doi.org/10.1016/j.biochi.2019.03.015.

[26] F. Angelucci, A.A. Sayed, D.L. Williams, G. Boumis, M. Brunori, D. Dimastrogiovanni, A.E. Miele, F. Pauly, A. Bellelli, Inhibition of Schistosoma mansoni thioredoxin-glutathione reductase by Auranofin: structural and kinetic aspects, J. Biol. Chem. 284 (42) (2009) 28977–28985, https://doi.org/10.1074/jbc.m109.020701.

[27] S. Han, K. Kim, H. Kim, J. Kwon, Y.-H. Lee, C.-K. Lee, Y. Song, S.-J. Lee, N. Ha, K. Kim, Auranofin inhibits overproduction of pro-inflammatory cytokines, cyclooxygenase expression and PGE2 production in macrophages, Arch Pharm. Res. (Seoul) 31 (1) (2008) 67–74, https://doi.org/10.1007/s12272-008-1122-9.

[28] N.-H. Kim, M.-Y. Lee, S.-J. Park, J.-S. Choi, M.-K. Oh, I.-S. Kim, Auranofin blocks interleukin-6 signalling by inhibiting phosphorylation of JAK1 and STAT3, Immunology 122 (4) (2007) 607–614, https://doi.org/10.1111/j.1365-2567.2007.02679.x.

[29] S.-J. Park, A.-N. Lee, H.-S. Youn, TBK1-Targeted suppression of TRIF-dependent signaling pathway of toll-like receptor 3 by auranofin, Arch Pharm. Res. (Seoul) 33 (6) (2010) 939–945, https://doi.org/10.1007/s12272-010-0618-2.

[30] E. Schuh, C. Pflüger, A. Citta, A. Folda, M.P. Rigobello, A. Bindoli, A. Casini, F. Mohr, Gold(I) carbene complexes causing thioredoxin 1 and thioredoxin 2 oxidation as potential anticancer agents, J. Med. Chem. 55 (11) (2012) 5518–5528, https://doi.org/10.1021/jm300428v.

[31] D. Oommen, D. Yiannakis, A.N. Jha, BRCA1 deficiency increases the sensitivity of ovarian cancer cells to auranofin, Mutat. Res. Fund Mol. Mech. Mutagen 784–785 (2016) 8–15, https://doi.org/10.1016/j.mrfmmm.2015.11.002.

[32] H. Huang, Y. Liao, N. Liu, X. Hua, J. Cai, C. Yang, H. Long, C. Zhao, X. Chen, X. Lan, D. Zang, J. Wu, X. Li, X. Shi, X. Wang, J. Liu, Two clinical drugs deubiquitinase inhibitor auranofin and aldehyde Dehydrogenase inhibitor disulfiram trigger synergistic anti-tumor effects in vitro and in vivo, Oncotarget 7 (3) (2016) 2796–2808, https://doi.org/10.18632/oncotarget.6425.

[33] S. Jia, R. Wang, K. Wu, H. Jiang, Z. Du, Elucidation of the mechanism of action for metal based anticancer drugs by mass spectrometry-based quantitative proteomics, Molecules 24 (3) (2019) 581, https://doi.org/10.3390/molecules24030581.

[34] H. Wang, Y. Zhou, X. Xu, H. Li, H. Sun, Metalloproteomics in conjunction with other omics for uncovering the mechanism of action of metallodrugs: mechanism-driven new therapy development, Curr. Opin. Chem. Biol. 55 (2020) 171–179, https://doi.org/10.1016/j.cbpa.2020.02.006.

[35] F. Magherini, A. Modesti, L. Bini, M. Puglia, I. Landini, S. Nobili, E. Mini, M. A. Cinellu, C. Gabbiani, L. Messori, Exploring the biochemical mechanisms of cytotoxic gold compounds: a proteomic study, J. Biol. Inorg. Chem. 15 (4) (2010) 573–582, https://doi.org/10.1007/s00775-010-0624-3.

[36] F. Guidi, I. Landini, M. Puglia, F. Magherini, C. Gabbiani, M.A. Cinellu, S. Nobili, T. Fiaschi, L. Bini, E. Mini, L. Messori, A. Modesti, Proteomic analysis of ovarian cancer cell responses to cytotoxic gold compounds, Metallomics 4 (3) (2012) 307–314, https://doi.org/10.1039/C2MT00083K.

[37] E. Hatem, S. Azzi, N. El Banna, T. He, A. Heneman-Masurel, L. Vernis, D. Baïlle, V. Masson, F. Dingli, D. Loew, B. Azzarone, P. Eid, G. Baldacci, M.-E. Huang, Auranofin/vitamin C: a novel drug combination targeting triple-negative breast cancer, J. Natl. Cancer Inst. (2018), https://doi.org/10.1093/jnci/djy149.

[38] Y.-M. Go, J.R. Roede, D.I. Walker, D.M. Duong, N.T. Seyfried, M. Orr, Y. Liang, K. D. Pennell, D.P. Jones, Selective targeting of the cysteine proteome by thioredoxin and glutathione redox systems, Mol. Cell. Proteomics 12 (11) (2013) 3285–3296, https://doi.org/10.1074/mcp.M113.030437.

[39] A.A. Saei, H. Gullberg, P. Sabatier, C.M. Beusch, K. Johansson, B. Lundgren, P. I. Arvidsson, E.S.J. Arnér, R.A. Zubarev, Comprehensive chemical proteomics for target deconvolution of the redox active, Drug Auranofin. Redox Biology 32 (2020) 101491, https://doi.org/10.1016/j.redox.2020.101491.

[40] I. Landini, L. Massai, D. Cirri, T. Gamberi, P. Paoli, L. Messori, E. Mini, S. Nobil, Structure-activity relationships in a series of auranofin analogues showing remarkable antiproliferative properties, J. Inorg. Biochem. 208 (2020) 111079, https://doi.org/10.1016/j.jinorgbio.2020.111079.

[41] N. Barraud, S. Létoffé, C. Beloin, J. Vinh, G. Chiappetta, J.M. Ghigo, Lifestyle-specific S-nitrosylation of protein cysteine thiols regulates Escherichia coli biofilm formation and resistance to oxidative stress, NPJ Biofilms Microbiomes 7 (1) (2021) 34, https://doi.org/10.1038/s41522-021-00203-w.

[42] S. Shakir, J. Vinh, G. Chiappetta, Quantitative analysis of the cysteine redoxome by iodoacetyl tandem mass tags, Anal. Bioanal. Chem. 409 (15) (2017) 3821–3830, https://doi.org/10.1007/s00216-017-0326-6.

[43] D.W. Huang, B.T. Sherman, R.A. Lempicki, Systematic and integrative analysis of large gene lists using DAVID Bioinformatics Resources, Nat. Protoc. 4 (1) (2009) 44–57, https://doi.org/10.1038/nprot.2008.211.

[44] L. Fagerberg, C. Stadler, M. Skogs, M. Hjelmare, K. Jonasson, M. Wiking, A. Abergh, M. Uhlén, E. Lundberg, Mapping the subcellular protein distribution in three human cell lines, J. Proteome Res. 10 (8) (2011) 3766–3777, https://doi.org/10.1021/pr200379a.

[45] C.K. Mirabelli, C.M. Sung, J.P. Zimmerman, D.T. Hill, S. Mong, S.T. Crooke, Interactions of gold coordination complexes with DNA, Biochem. Pharmacol. 35 (9) (1986) 1427–1433, https://doi.org/10.1016/0006-2952(86)90106-1, 1;.

[46] X. Liu, W. Wang, Y. Yin, M. Li, H. Li, H. Xiang, A. Xu, X. Mei, B. Hong, W. Lin, A high-throughput drug screen identifies Auranofin as a potential sensitizer of cisplatin in small cell lung cancer, Invest. N. Drugs 37 (6) (2019) 1166–1176, https://doi.org/10.1007/s10637-019-00750-2.

[47] M. Auranofin Yamashita, Past to present, and repurposing, Int. Immunopharm. 101 (Pt B) (2021) 108272, https://doi.org/10.1016/j.intimp.2021.108272.

[48] S.B. Wall, R. Li, B. Butler, A.R. Burg, H.M. Tse, J.L. Larson-Case, A.B. Carter, C. J. Wright, L.K. Rogers, T.E. Tipple, Auranofin-mediated NRF2 induction attenuates interleukin 1 beta expression in alveolar macrophages, Antioxidants 10 (5) (2021) 632, https://doi.org/10.3390/antiox10050632.

[49] K. Dunigan, Q. Li, R. Li, M.L. Locy, S. Wall, T.E. Tipple, The thioredoxin reductase inhibitor auranofin induces heme oxygenase-1 in lung epithelial cells via Nrf2-dependent mechanisms, Am. J. Physiol. Lung Cell Mol. Physiol. 315 (4) (2018) L545–L552, https://doi.org/10.1152/ajplung.00214.2018.

[50] T. Gamberi, G. Chiappetta, T. Fiaschi, A. Modesti, F. Sorbi, F. Magherini, Upgrade of an old drug: auranofin in innovative cancer therapies to overcome drug resistance and to increase drug effectiveness, Med. Res. Rev. (2021), https://doi.org/10.1002/med.21872. *In press*.

[51] I. Soylu, S.M. Marino, Cpipe: a comprehensive computational platform for sequence and structure-based analyses of Cysteine residues, Bioinformatics 33 (15) (2017) 2395–2396, https://doi.org/10.1093/bioinformatics/btx181.

[52] H.K. Heileen, Stability of Metal−Glutathione complexes during oxidation by hydrogen peroxide and Cu (II)-Catalysis, Environ. Sci. Technol. 41 (7) (2007) 2338–2342, https://doi.org/10.1021/es062269+.

[53] A. Chernobrovkin, C. Marin-Vicente, N. Visa, R.A. Zubarev, Functional Identification of Target by Expression Proteomics (FITExP) reveals protein targets and highlights mechanisms of action of small molecule drugs, Sci. Rep. 5 (2015) 11176, https://doi.org/10.1038/srep11176.

[54] J.J. Skoko, S. Attaran, C.A. Neumann, Signals getting crossed in the entanglement of redox and phosphorylation pathways: phosphorylation of peroxiredoxin proteins sparks, Cell Signaling. Antioxidants (Basel) 8 (2) (2019) 29, https://doi.org/10.3390/antiox8020029.

[55] W. Xu, S. Wang, Q. Chen, Y. Zhang, P. Ni, X. Wu, J. Zhang, F. Qiang, A. Li, O. D. Røe, S. Xu, M. Wang, R.E. Zhang, J. Zhou, TXNL1-XRCC1 pathway regulates cisplatin-induced cell death and contributes to resistance in human gastric cancer, Cell Death Dis. 5 (2) (2014) e1055, https://doi.org/10.1038/cddis.2014.27.

[56] V. Ghini, T. Senzacqua, T. Massai, T. Gamberi, L. Messori, P. Turano, NMR reveals the metabolic changes induced by Auranofin in A2780 cancer cells: evidence for glutathione dysregulation, Dalton Trans. 50 (18) (2021) 6349–6355.

[57] D.M. Townsend, K.D. Tew, The role of glutathione-S-transferase in anti-cancer drug resistance, Oncogene 22 (47) (2003) 7369–7375, https://doi.org/10.1038/sj.onc.1206940.

[58] P. Tangkhuenkhan, K. Harncharoen, S. Thanasitthichai, D. Tiwawech, W. Purisa, P. Saelee, R. Wattanalai, Frequency and association of GSTM1 and GSTT1 gene polymorphisms with survival in breast cancer patients, Asian Pac. J. Cancer Prev. APJCP 21 (8) (2020) 2251–2257, https://doi.org/10.31557/apjcp.2020.21.8.2251.

[59] T. Yumnamcha, T.S. Devi, L.P. Singh, Auranofin mediates mitochondrial dysregulation and inflammatory cell death in human retinal pigment epithelial cells: implications of retinal neurodegenerative diseases, Front. Neurosci. 13 (2019) 1065, https://doi.org/10.3389/fnins.2019.01065.

[60] C. Cirotti, S. Rizza, P. Giglio, N. Poerio, M.F. Allega, G. Claps, C. Pecorari, J. H. Lee, B. Benassi, D. Barilà, C. Robert, J.S. Stamler, F. Cecconi, M. Fraziano, T. T. Paull, G. Filomeni, Redox activation of ATM enhances GSNOR translation to sustain mitophagy and tolerance to oxidative stress, EMBO Rep 22 (1) (2021), e50500, https://doi.org/10.15252/embr.202050500.

[61] F. Radenkovic, O. Holland, J.J. Vanderlelie, A.V. Perkins, Selective inhibition of endogenous antioxidants with Auranofin causes mitochondrial oxidative stress which can be countered by selenium supplementation, Biochem. Pharmacol. 146 (2017) 42–52, https://doi.org/10.1016/j.bcp.2017.09.009.

[62] B. Bhattacharya, Mohd Omar, M.F, R. Soong, The Warburg effect and drug resistance, Br. J. Pharmacol. 173 (6) (2016) 970–979, https://doi.org/10.1111/bph.13422.

[63] S. Yoshida, S. Tsutsumi, G. Muhlebach, C. Sourbier, M.J. Lee, S. Lee, E. Vartholomaiou, M. Tatokoro, K. Beebe, N. Miyajima, R.P. Mohney, Y. Chen, H. Hasumi, W. Xu, H. Fukushima, K. Nakamura, F. Koga, K. Kihara, J. Trepel, D. Picard, L. Neckers, Molecular chaperone TRAP1 regulates a metabolic switch between mitochondrial respiration and aerobic glycolysis, Proc. Natl. Acad. Sci. U. S. A. 110 (17) (2013) E1604–E1612, https://doi.org/10.1073/pnas.1220659110.

[64] S. Rizza, C. Montagna, S. Cardaci, E. Maiani, G. Di Giacomo, V. Sanchez-Quiles, B. Blagoev, A. Rasola, D. De Zio, J.S. Stamler, F. Cecconi, G. Filomeni, S-nitrosylation of the mitochondrial chaperone TRAP1 sensitizes hepatocellular carcinoma cells to inhibitors of succinate Dehydrogenase cancer, Res 76 (4) (2016) 4170–4182, https://doi.org/10.1158/0008-5472.can-15-2637.

[65] F. Faienza, M. Lambrughi, S. Rizza, C. Pecorari, P. Giglio, J. Salamanca Viloria, M. F. Allega, G. Chiappetta, J. Vinh, F. Pacello, A. Battistoni, A. Rasola, E. Papaleo, G. Filomeni, S-nitrosylation affects TRAP1 structure and ATPase activity and modulates cell response to apoptotic stimuli, Biochem. Pharmacol. 176 (2020) 113869, https://doi.org/10.1016/j.bcp.2020.113869.

[66] S. Hofmann, U. Rothbauer, N. Muehlenbein, K. Baiker, K. Hell, M.F. Bauer, Functional and mutational characterization of human MIA40 acting during import into the mitochondrial intermembrane space, J. Mol. Biol. 353 (2005) 517–528, https://doi.org/10.1016/j.jmb.2005.08.064.

[67] K. Hell, The Erv1–Mia40 disulfide relay system in the intermembrane space of mitochondria, Biochim. Biophys. Acta 783 (4) (2008) 601–609, https://doi.org/10.1016/j.bbamcr.2007.12.005.

[68] C. Reinhardt, G. Arena, K. Nedara, R. Edwards, C. Brenner, K. Tokatlidis, N. Modjtahedi, AIF meets the CHCHD4/Mia40-dependent mitochondrial import pathway, Biochim. Biophys. Acta (BBA) - Mol. Basis Dis. 1866 (6) (2020) 165746, https://doi.org/10.1016/j.bbadis.2020.165746.

[69] R.G. Kranz, R. Richard-Fogal, J.T. Taylor, E.R. Frawley, Cytochrome c biogenesis: mechanisms for covalent modifications and trafficking of heme and for heme-iron redox control, Microbiol. Mol. Biol. Rev. 73 (3) (2009) 510–528, https://doi.org/10.1128/mmbr.00001-09.

[70] H. Steiner, G. Kispal, A. Zollner, A. Haid, W. Neupert, R. Lill, Heme binding to a conserved Cys-Pro-Val motif is crucial for the catalytic function of mitochondrial heme lyases, J. Biol. Chem. 271 (1996) 32605–32611, https://doi.org/10.1074/jbc.271.51.32605.

[71] M.P. Rigobello, G. Scutari, R. Boscolo, A. Bindoli, Induction of mitochondrial permeability transition by Auranofin, a Gold(I)-phosphine derivative, Br. J. Pharmacol. 136 (2002) 1162, https://doi.org/10.1038/sj.bjp.0704823.

[72] Y. Zheng, Y. Shi, C. Tian, C. Jiang, H. Jin, C. Chen, A. Almasan, H. Tang, Q. Chen, Essential role of the voltage-dependent anion channel (VDAC) in mitochondrial permeability transition pore opening and cytochrome c release induced by arsenic trioxide, Oncogene 23 (6) (2004) 1239–1247, https://doi.org/10.1038/sj.onc.1207205.

[73] J.V. Olsen, M. Vermeulen, A. Santamaria, C. Kumar, M.L. Miller, L.J. Jensen, F. Gnad, J. Cox, T.S. Jensen, E.A. Nigg, S. Brunak, M. Mann, Quantitative phosphoproteomics reveals widespread full phosphorylation site occupancy during mitosis, Sci. Signal. 3 (104) (2010 Jan 12), https://doi.org/10.1126/scisignal.2000475 ra3.

[74] T.T. Nguyen, M.V. Stevens, M. Kohr, C. Steenbergen, M.N. Sack, E. Murphy, Cysteine 203 of Cyclophilin D is critical for Cyclophilin D activation of the mitochondrial permeability transition pore, J. Biol. Chem. 286 (46) (2011) 40184–40192, https://doi.org/10.1074/jbc.m111.243469.

[75] S. Shanmughapriya, S. Rajan, N.E. Hoffman, A.M. Higgins, D. Tomar, N. Nemani, K.J. Hines, D.J. Smith, A. Eguchi, S. Vallem, F. Shaikh, M. Cheung, N.J. Leonard, R.S. Stolakis, M.P. Wolfers, J. Ibetti, J.K. Chuprun, N.R. Jog, S.R. Houser, W. J. Koch, J.W. Elrod, M. Madesh, SPG7 is an essential and conserved component of the mitochondrial permeability transition pore, Mol. Cell. 60 (1) (2015) 47–62, https://doi.org/10.1016/j.molcel.2015.08.009.

[76] S. Montessuit, S.P. Somasekharan, O. Terrones, S. Lucken-Ardjomande, S. Herzig, R. Schwarzenbacher, D. Manstein, E. Bossy-Wetzel, G. Basañez, P. Meda, J. C. Martino, Membrane remodeling induced by the dynamin related protein Drp1 stimulates Bax oligomerization, Cell 142 (6) (2010) 889–901, https://doi.org/10.1016/j.cell.2010.08.017.

[77] C. Kumar, A. Igbaria, B. D'Autreaux, A.G. Planson, C. Junot, E. Godat, A. K. Bachhawat, A. Delaunay-Moisan, M.B. Toledano, Glutathione revisited: a vital function in iron metabolism and ancillary role in thiol-redox control, EMBO J 30 (2011) 2044–2056, https://doi.org/10.1038/emboj.2011.105.

[78] G.J. Poet, O.B.V. Oka, M. van Lith, Z. Cao, P.J. Robinson, M.A. Pringle, E.S. J. Arnér, N.J. Bulleid, Cytosolic thioredoxin reductase 1 is required for correct disulfide formation in the ER, EMBO J. 36 (5) (2017) 693–702, https://doi.org/10.15252/embj.201695336.

[79] C. Guerra, G. Brambilla Pisoni, T. Solda, M. Molinari, The reductase TMX1 contributes to ERAD by preferentially acting on membrane-associated folding-defective polypeptides, Biochem. Biophys. Res. Commun. 503 (2018) 938–943, https://doi.org/10.1016/j.bbrc.2018.06.099.

[80] A. Raturi, T. Gutiérrez, C. Ortiz-Sandoval, A. Ruangkittisakul, M.S. Herrera-Cruz, J.P. Rockley, K. Gesson, D. Ourdev, P.H. Lou, E. Lucchinetti, N. Tahbaz, M. Zaugg, S. Baksh, K. Ballanyi, T. Simmen, TMX1 determines cancer cell metabolism as a

thiol-based modulator of ER–mitochondria Ca2+ flux, J. Cell Biol. 214 (4) (2016) 433–444, https://doi.org/10.1083/jcb.201512077.
[81] Y. Matsuo, K. Hirota, Transmembrane thioredoxin-related protein TMX1 is reversibly oxidized in response to protein accumulation in the endoplasmic reticulum, FEBS Open Bio 7 (11) (2017) 1768–1777, https://doi.org/10.1002/2211-5463.12319.
[82] S. Schulman, B. Wang, W. Li, T.A. Rapoport, Vitamin K epoxide reductase prefers ER membrane-anchored thioredoxin-like redox partners, Proc. Natl. Acad. Sci. Unit. States Am. 107 (34) (2010) 15027–15032, https://doi.org/10.1073/pnas.1009972107.
[83] D. Eletto, E. Chevet, Y. Argon, C. Appenzeller-Herzog, Redox controls UPR to control redox, J. Cell Sci. 127 (2014) 3649–3658, https://doi.org/10.1242/jcs.153643.
[84] B. Gess, K.H. Hofbauer, R.H. Wenger, C. Lohaus, H.E. Meyer, A. Kurtz, The cellular oxygen tension regulates expression of the endoplasmic oxidoreductase ERO1-Lalpha, Eur. J. Biochem. 270 (10) (2003) 2228–2235, https://doi.org/10.1046/j.1432-1033.2003.03590.x.
[85] E. Avzov, B.C.S. Cross, G.S. Kaminski Schierle, M. Winters, H.P. Harding, E. Pinho Melo, C.F. Kaminski, D. Ron, J. Cell Biol. 201 (2) (2013) 337–349, https://doi.org/10.1083/jcb.201211155.
[86] Y. Li, P. Camacho, Ca2+-dependent redox modulation of SERCA 2b by ERp57, J. Cell Biol. 164 (1) (2004) 35–46, https://doi.org/10.1083/jcb.200307010.
[87] R. Ushioda, A. Miyamoto, M. Inoue, S. Watanabe, M. Okumura, K.I. Maegawa, K. Uegaki, S. Fujii, Y. Fukuda, M. Umitsu, J. Takagi, K. Inaba, K. Mikoshiba, K. Nagata, Redox-assisted regulation of Ca2+ homeostasis in the endoplasmic reticulum by disulfide reductase ERdj5, Proc. Natl. Acad. Sci. U. S. A. 113 (41) (2016) E6055–E6063. https://doi: 10.1073/pnas.1605818113.
[88] T. Anelli, L. Bergamelli, E. Margittai, A. Rimessi, C. Fagioli, A. Malgaroli, P. Pinton, M. Ripamonti, R. Rizzuto, R. Sitia, Ero1a regulates Ca(2+) fluxes at the endoplasmic reticulum-mitochondria interface (MAM), Antioxidants Redox Signal. 16 (2012) 1077–1087, https://doi.org/10.1089/ars.2011.4004.
[89] P.K. Sobhan, M. Seervi, L. Deb, S. Varghese, A. Soman, J. Joseph, K.A. Mathew, G. Raghu, G. Thomas, E. Sreekumar, S. Manjula, T.R. Santosh Kumar, Calpain and reactive oxygen species targets Bax for mitochondrial permeabilisation and caspase activation in zerumbone induced apoptosis, PLoS One 8 (4) (2013 Apr 9), e59350, https://doi.org/10.1371/journal.pone.0059350.
[90] L. Scorrano, S.A. Oakes, J.T. Opferman, E.H. Cheng, M.D. Sorcinelli, T. Pozzan, S. J. Korsmeyer, BAX and BAK regulation of endoplasmic reticulum Ca2+: a control point for apoptosis, Science 300 (5616) (2003) 135–139, https://doi.org/10.1126/science.1081208.
[91] J. Korsmeyer, M.C. Wei, M. Saito, S. Weiler, K.J. Oh, P.H. Schlesinger, Pro-apoptotic cascade activates BID, which oligomerizes BAK or BAX into pores that result in the release of cytochrome c, Cell Death Differ 7 (12) (2000) 1166–1173, https://doi.org/10.1038/sj.cdd.4400783.
[92] A. Gross, X.M. Yin, K. Wang, M.C. Wei, J. Jockel, C. Milliman, H. Erdjument-Bromage, P. Tempst, S.J. Korsmeyer, Caspase cleaved BID targets mitochondria and is required for cytochrome c release, while BCL-XL prevents this release but not tumor necrosis factor-R1/fas, J. Biol. Chem. 274 (2) (1999) 1156–1163, https://doi.org/10.1074/jbc.274.2.1156.
[93] K. Zhang, H. Liu, Z. Song, Y. Jiang, H. Kim, L. Samavati, H.M. Nguyen, Z.Q. Yang, The UPR transducer IRE1 promotes breast cancer malignancy by degrading tumor suppressor microRNAs, iScience 23 (9) (2020) 101503, https://doi.org/10.1016/j.isci.2020.101503.
[94] I. Landini, A. Lapucci, A. Pratesi, L. Massai, C. Napoli, G. Perrone, P. Pinzani, L. Messori, E. Mini, S. Nobili, Selection and characterization of a human ovarian cancer cell line resistant to auranofin, Oncotarget 8 (56) (2017) 96062–96078, https://doi.org/10.18632/oncotarget.21708.
[95] B.R. You, W.H. Park, Auranofin induces mesothelioma cell death through oxidative stress and GSH depletion, Oncol. Rep. 35 (1) (2016) 546–551, https://doi.org/10.3892/or.2015.4382.
[96] B.R. You, H.R. Shin, B.R. Han, S.H. Kim, W.H. Park, Auranofin induces apoptosis and necrosis in HeLa cells via oxidative stress and glutathione depletion, Mol. Med. Rep. 11 (2) (2015) 1428–1434, https://doi.org/10.3892/mmr.2014.2830.
[97] S. Vaughan, J.I. Coward, r.C.Jr Bast, A. Berchuck, J.S. Berek, J.D. Brenton, G. Coukos, C.C. Crum, R. Drapkin, D. Etemadmoghadam, M. Friedlander, H. Gabra, S.B. Kaye, C.J. Lord, E. Lengyel, D.A. Levine, I.A. McNeish, U. Menon, G.B. Mills, K.P. Nephew, A.M. Oza, A.K. Sood, E.A. Stronach, H. Walczak, D. D. Bowtell, F.R. Balkwill, Rethinking ovarian cancer: recommendations for improving outcomes, Nat. Rev. Cancer 11 (10) (2011) 719–725, https://doi.org/10.1038/nrc3144.
[98] I. Masgras, C. Sanchez-Martin, G. Colombo, A. Rasola, The chaperone TRAP1 as a modulator of the mitochondrial adaptations in cancer cells, Front. Oncol. 7 (2017) 58, https://doi.org/10.3389/fonc.2017.00058M.
[99] F. addalena, V. Condelli, D. Swann Matassa, C. Pacelli, R. Scrima, G. Lettini, V. Li Bergolis, M. Pietrafesa, F. Crispo, A. Piscazzi, G. Storto, N. Capitanio, F. Esposito, M. Landriscina, TRAP1 enhances Warburg metabolism through modulation of PFK1 expression/activity and favors resistance to EGFR inhibitors in human colorectal carcinomas, Mol Oncol 14 (12) (2020) 3030–3047, https://doi.org/10.1002/1878-0261.12814.
[100] P. Zou, M. Chen, J. Ji, W. Chen, X. Chen, S. Ying, J. Zhang, Z. Zhang, Z. Liu, S. Yang, G. Liang, Auranofin induces apoptosis by ROS-mediated ER stress and mitochondrial dysfunction and displayed synergistic lethality with piperlongumine in gastric cancer, Oncotarget 6 (34) (2015) 36505–36521, https://doi.org/10.18632/oncotarget.5364.
[101] W. Fiskus, N. Saba, N. Shen, M. Ghias, J. Liu, S. Das Gupta, L. Chauhan, R. Rao, S. Gunewardena, K. Schorno, C.P. Austin, K. Maddocks, J. Byrd, A. Melnick, P. Huang, A. Wiestner, K.N. Bhalla, Auranofin induces lethal oxidative and endoplasmic reticulum stress and exerts potent preclinical activity against chronic lymphocytic leukemia, Cancer Res. 74 (9) (2014) 2520–2532, https://doi.org/10.1158/0008-5472.can-13-2033.